Seismic resilience of typical steel school building and retrofitting options based on FEMA P-58 under mainshock-aftershock effects

Authors: Kimia Koohfallah[a]; Morteza Raissi Dehkordi[b]; Dina D'Ayala[c]; Gholamreza Ghodrati Amiri[d]; Mahdi Eghbali[e]; Delbaz Samadian[f]*

[a] *Graduate MSc, School of Civil Engineering, Iran University of Science and Technology, Tehran, Iran.* (kimia_koohfallah@alumni.iust.ac.ir)

[b]*Associate Professor, Natural Disasters Prevention Research Center, School of Civil Engineering, Iran University of Science and Technology, Tehran, Iran.* (mraissi@iust.ac.ir)

[c] *Professor, Department of Civil, Environment & Geomatic Engineering Faculty of Engineering Science, 113, UCL Chadwick Building, Gower Street, London, WC1E 6BT.* (d.dayala@ucl.ac.uk)

[c]*Professor, Natural Disasters Prevention Research Center, School of Civil Engineering, Iran University of Science and Technology, Tehran, Iran.* (Ghodrati@iust.ac.ir)

[*e]*(Corresponding author) Assistant Professor, Structural Hybrid Simulation Research Lab, Department of Civil Engineering, Faculty of Engineering, University of Zanjan, Zanjan, Iran.* (eghbali@znu.ac.ir)

[f] *Graduate MSc, School of Civil Engineering, Department of Structural Engineering, Semnan University, Semnan, Iran.* (delbazamad70@semnan.ac.ir)

Abstract

This paper investigates the selection of the appropriate retrofitting option for a steel school building based on the resilience index with FEMA P-58 methodology and considers different scenarios of mainshock-aftershock (MS-AS) effects. A typical high school in Kermanshah, Iran, and its two retrofitting options, including retrofitting with concentric braces and retrofitting with shear walls, have been selected as a case study, and their resilience indexes have been evaluated at two hazard levels of 2% and 10% in 50 years. In order to calculate the resilience index, seismic damage, repair cost, and repair time of existing school and retrofitting options are evaluated by FEMA P-58 methodology through PACT software. In this study, the effect of the damage level of the mainshock on the total damage of the MS-AS sequences is considered, and the different levels of damage caused by the mainshock are expressed in terms of the maximum inter-story drift ratio (IDR). So in this research, to indicate the mainshock damage on the structure, the response levels of 0.007, 0.025, and 0.05 IDR values have been considered. Investigation of the MS-AS effects on the seismic resilience index of schools shows that the increase in mainshock damage, which is associated with an increase in repair cost and repair time, leads to a reduction in the resilience index of the structures. In this study, the resilience index of the existing school at hazard level 1 has increased from 0.6206 to 0.6916 for the retrofitting with concentric braces and to 0.9620 for shear walls, respectively. Also, at hazard level 2, the resilience index of the existing school has increased from zero to 0.5604 and 0.9287 in retrofitting options with concentric braces and shear walls, respectively. This increase in the resilience indexes shows the positive effect of retrofitting on the seismic performance of the schools. In addition, it was determined that the retrofitting option with shear walls has less repair time and repair cost compared to another option in both hazard levels, so it is finally selected as the appropriate retrofitting option.

Keywords

Seismic Resilience; School Buildings; FEMA P-58; Functionality Curve; Mainshock-Aftershock.

1. Introduction

Over the past few decades, the rapid expansion of urban areas and the establishment of urban regions with lower standards, particularly in developing nations, have rendered them increasingly susceptible to both human-induced and natural crises (Odabaşi et al. 2020). With more than half of the global population now residing in urban areas, the risks associated with these locations have escalated as settlements and other man-made structures are increasingly exposed to environmental and tectonic hazards. Recent disasters serve as evidence that communities and individuals are becoming more vulnerable, with risks on the rise (Ranjbar and Naderpour 2020); (De Martino et al. 2017); (Miranda et al. 2012). The historical record of earthquakes demonstrates that their impact on society far exceeds the physical damage inflicted on buildings, necessitating significant efforts to restore society to its pre-disaster state. This becomes even more critical when these events surpass the assumptions and regulations outlined in the design standards upon which the infrastructure was built (Rajabpour 2018). In recent years, the importance of fostering disaster-resilient societies has gained recognition within the field of Crisis Management (Cimellaro et al. 2016); (Chang et al. 2004).

The resilience framework proposed by Bruneau et al. (2003) is founded on the belief that a decline in performance following a hazardous event is inevitable. To effectively respond to such events, it is crucial to identify and mitigate the vulnerabilities present within the system. In recent times, communities worldwide have directed their attention towards addressing and finding solutions for catastrophic events. This concept has gained significant traction in societies that acknowledge the impossibility of completely recognizing and predicting risks. Instead, the focus is on adapting to and managing these risks to minimize their impact on human lives (Renschler et al., 2011). Resilience, as a concept, extends beyond structures and encompasses systems and societies as well (van der Leeuw and Aschan-Leygonie, 2005; Kendra and Wachtendorf, 2003; Paton et al., 2000; Home and Orr, 1997). Assessing the resilience of structures quantitatively can serve as a valuable step in determining the appropriate course of action to enhance community safety (Klein et al., 2003). Crisis management and identifying societal weaknesses in the face of future disasters are crucial aspects associated with the concept of resilience.

Cimellaro et al. (2016) have expanded the conventional resilience framework by introducing seven dimensions, namely Population, Environmental/Ecosystem, Organized Governmental Services, Physical Infrastructure, Lifestyle and Community Competence, Economic Development, and Social-Cultural Capital, collectively referred to as PEOPLES. This broader approach considers these dimensions as the basis for integrating quantitative or qualitative models that measure the resilience of a system to severe events or disasters.

Joyner and Sasani (2020) conducted a study to analyze the seismic resilience of structures. Their objective was to enhance the comprehension of the fundamental relationships that influence building performance, with the ultimate aim of facilitating the development of regulations focused on structural performance. In a similar vein, Kurth et al. (2019) explored the concept of resilience within the US construction industry. The overarching goal of this industry is to strike a balance between the advantages of building production and the associated risks and rewards for various stakeholders, including owners, designers, engineers, contractors, managers, investors, insurance companies, and tenants. Consequently, it is imperative to maintain an equilibrium between the benefits of construction and the expenses incurred in enhancing resilience.

Due to the significance of resilience in school buildings, which are essential structures within communities, numerous contributions have been made in this field. In Iran, Samadian et al. (2019) conducted a study to investigate the seismic resilience index of a concrete school building before and after seismic rehabilitation using shear walls. They utilized vulnerability curves to calculate the resilience index, which demonstrated higher accuracy compared to resilience indexes based solely on fragility functions. Another study by Samadian et al. (2020) explored the structural and non-structural damages of schools in the Kermanshah province following the Ezgeleh earthquake. Subsequently, an evidence-based seismic resilience index was estimated by Eghbali et al. (2020). Their findings concluded that retrofitting school buildings prior to earthquakes leads to improved seismic performance and increases the resilience index, bringing it closer to 100%. Shamsoddini-Motlagh et al. (2020) investigated the impact of carbonate corrosion on the seismic resilience of school buildings. They employed a loss function derived from vulnerability curves to extract the resilience index of the school structures. The results of their study indicated that corroded school buildings had lower resilience indexes at all hazard levels. Ekhlaspoor et al. (2022) developed a web-based software tool called Resilience Indicator (Ri), which can evaluate the seismic resilience index of Iranian structures. In the context of steel school structures in Iran, Sardari et al. (2020) selected the best seismic retrofit strategy through reliability and resiliency analysis. Similarly, other researchers have focused on the resilience and vulnerability assessment of school buildings worldwide, including Vatteri et al. (2022), Ruiz-García et al. (2021), D'Ayala et al. (2020), and De Angelis and Pecce (2015). Furthermore, studies have also emphasized the evaluation of resilience in other structures, such as those conducted by Niazi et al. (2021), Mokhtari and Naderpour (2020), Hosseinzadeh and Galal (2020a), and Cimellaro and Piqué (2016).

Federal Emergency Management Agency (FEMA P-58-1 (2018)) has recently provided solutions for the development of performance-based seismic design, as evidenced by several studies conducted in this field. For instance, Perrone et al. (2020) calculated the seismic loss assessment of three school buildings in Italy using the FEMA P-58 methodology. Similarly, Baker et al. (2016) evaluated the total downtime of 10 damaged buildings under the effect of the Canterbury 2010-2011 seismic sequence using the same methodology. Terzic et al. (2021) presented a framework for evaluating building performance after a seismic event, repair time of building, and mobilization time in starting recovery operations, all using the FEMA P-58 methodology. Furthermore, Terzic et al. (2019) investigated the effect of using different analytical models for reinforced concrete shear walls on the seismic performance of three types of structures, evaluating the damage and the repair time of the damaged components of the buildings via the FEMA P-58 methodology.

To adequately assess the impact of aftershocks on structures, it is essential to incorporate mainshock-aftershock sequences into seismic analyses. Typically, a mainshock event is followed by a series of aftershocks, which can result in significant structural damage, even if the mainshock itself only caused minor harm (Li et al., 2014). Aftershocks can occur within a range of minutes to several months after the mainshock (Scholz, 2002). When the time interval between an aftershock and the mainshock is short, there may not be sufficient time to repair the damaged structures before the subsequent aftershock occurs. Consequently, the cumulative damage to structures can be amplified by aftershocks (Naderpour and Vakili, 2019). In essence, the damage inflicted by the mainshock weakens the structures, making them more susceptible to collapse during subsequent aftershocks (Jalali et al., 2021). Numerous studies have been conducted in the field of seismic sequences, with some of them being referenced here. Wen et al. (2019) demonstrated that incorporating aftershocks into the seismic analysis increases the seismic demand on structures compared to considering only the mainshock. Therefore, when evaluating the resilience of a system, it is more appropriate to consider the complete seismic sequence. Putrino and D'Ayala (2019) proposed an iterative method that integrates failure mechanism analysis and the N2 method (Dolsek and Fajfar, 2005) to account for residual strength and ductility capacities after the mainshock. This approach was applied to two towns in Italy affected by the Central Italy 2016 earthquake (D'Ayala et al., 2016) to elucidate the observed distribution of damage in reality.

In the present study, a high school in Kermanshah-Iran, and its two retrofitting options have been selected to evaluate the resilience index using the FEMA P-58 methodology and considering the effects of different scenarios of mainshock-aftershock. The total damage of the structure in seismic sequences is affected by the initial damage caused by the mainshock. Hence, one of the goals of the present study is to explore the effects of different damage levels of the mainshock on the resilience index of the structures. This approach is novel not just within the Iranian context, where the FEMA P-58 methodology and the Performance Assessment Calculation Tool (PACT) (FEMA P-58-2 [31]) have not been previously applied, but also within the field of study of school infrastructure resilience where the effect of seismic sequence on resilience index has not been previously considered to the authors' knowledge. The outline of the paper is as follows. In Section

2, the methodology of the study is explained. In Section 3, the existing school and its retrofitting options are described while Section 4 describes the modeling of the schools and seismic analysis done by OpenSees V.3.2.0 (2020) software. In Section 5, the seismic damage assessment of schools calculated by PACT and FEMA P-58 methodology is presented. In Section 6, the functionality curves of the schools are presented and the resilience index is calculated.

2. Methodology

According to **Fig. 1**, which is the methodology followed in this work, the steps performed in this research are presented to evaluate the seismic resilience index. The first step is the selection of a case study. A high school in Iran in the city of Kermanshah and its two retrofitting options are selected. The selected school is built on soil type III according to the Iranian seismic code, standard NO.2800 (BHRC 2015). However, the seismic hazard analysis for soil type III in Kermanshah-Iran has not been performed, and for the purposes of this study, the seismic resilience is evaluated in two hazard levels including 10% and 2% in 50 years. Hence, the corresponding values (10% and 2% in 50 years) for each hazard level are obtained based on standard NO.2800. Also, to calculate the earthquake coefficient (C), based on the mentioned standard, the city of Kermanshah-Iran is located in a zone with a high seismicity level. Therefore, the design-based acceleration (A) is equal to 0.3g, schools are considered in the group of buildings with high importance, and their importance coefficient (I) is equal to 1.2.

In the next step, the existing building and its two retrofitting options are modeled in OpenSees software (McKenna and Fenves 2020). 32 mainshock-aftershock seismic sequences for seismic analysis are selected. Incremental Dynamic Analysis (IDA) with the “Hunt-Fill” algorithm (Vamvatsikos and Cornell 2001); (Vamvatsikos and Cornell 2002) has been adopted for seismic analysis.

In the next step, the Performance Assessment Calculation Tool (PACT) (FEMA P-58-2), developed as part of the FEMA P-58 methodology, is used to calculate loss estimation for the existing school and its two retrofitting options. FEMA P-58 is a methodology for developing a new generation of performance-based seismic design guidelines for buildings (FEMA P-58-1 [32]). PACT has fragility and consequence functions in its library, that performs loss calculation described in the FEMA P-58 methodology. The repair time and repair cost are extracted by modeling schools in the PACT tool. Then to evaluate the resilience index, the delay time at the beginning of the recovery process after the earthquake event is calculated by two procedures (the organization for Development, Renovation and Equipping Schools of Iran (DRES) method and REDi guideline (Almufti and Willford, 2013)). Next, functionality curves are obtained by loss of schools, repair time and delay time at the beginning of the recovery process. Finally, the resilience index for the existing school and its retrofitting options, are extracted and the appropriate option for retrofitting this school is selected based on the seismic resilience index as well.

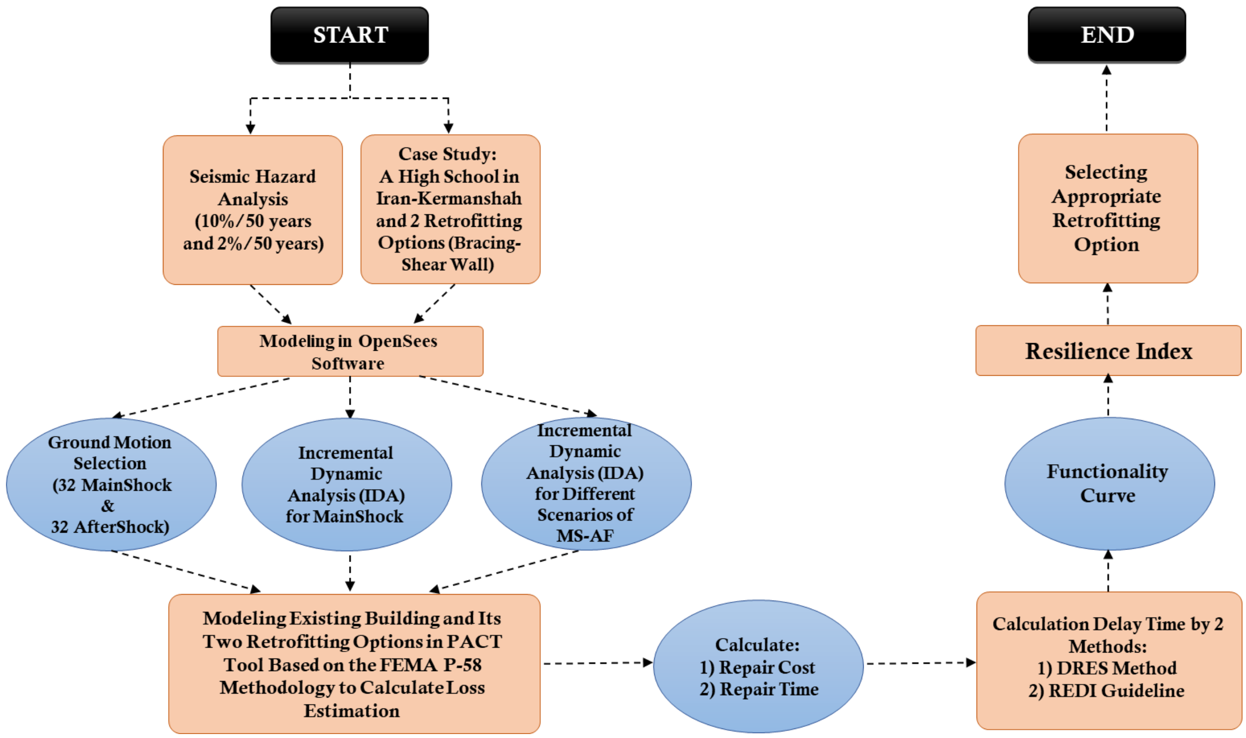

Fig. 1. The methodology to select an appropriate retrofitting option by resilience index in this study.

3. Case Study

Schools are one of the critical structures in any community because children spend long hours in schools. Therefore, schools should be usually designed to be available for immediate occupancy following a seismic event, in other words, they should be designed to perform in such a way that students' and staff's safety can be ensured and that they can be used as an emergency center immediately after an earthquake (FEMA P-424 [61]). Under some seismic codes, it might be required for schools to be immediately operational after an earthquake (FEMA P-424), however, in most countries, schools are classified as public buildings, but not as essential facilities. According to standard NO.2800, schools are classified in the group of vital structures and they should be designed to maintain their stability at life safety performance level (LS) at a hazard level of 10% over 50 years. Therefore, in this study, the proposed options for retrofitting the existing school are designed in such a way that the school should remain stable for LS performance level under the 10%/50 years hazard level.

In this study, to illustrate the methodology presented in Section 2, a case study of a typical high school and its rehabilitation options have been selected from the DRES database. The school building consists of 3 floors (ground floor, first and second) and is made of steel frame. The total area and total height of the school are 1920 m^2 and 10.20 m, respectively. Its lateral resisting system is implemented as concentric braces in both directions (B, D, F, and K frames in N-S direction; 2 and 5 frames in E-W direction). The fixity conditions between structural elements are pinned-based connections. This school was built in 1987 in Sarpole-Zahab, Kermanshah, Iran on soil type III according to the definition of standard NO.2800. From the results of the analysis of this school, it can be concluded that the structure is regular in plan and height owing to the coincidence of the mass center and rigidity center of the structure. The view and plan view of the existing school are presented in **Figs. 2(a)** and **(b)**. In the following, the pertinent details of the existing school are provided.

(a)

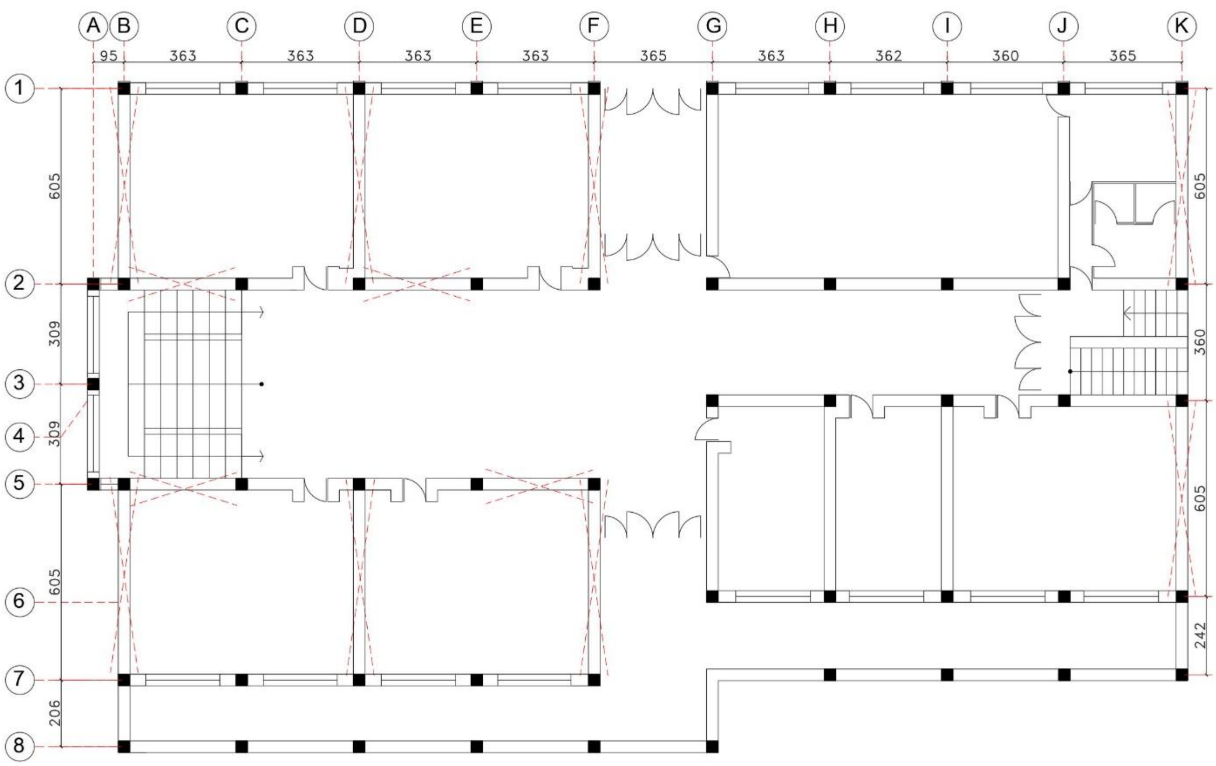

(b)

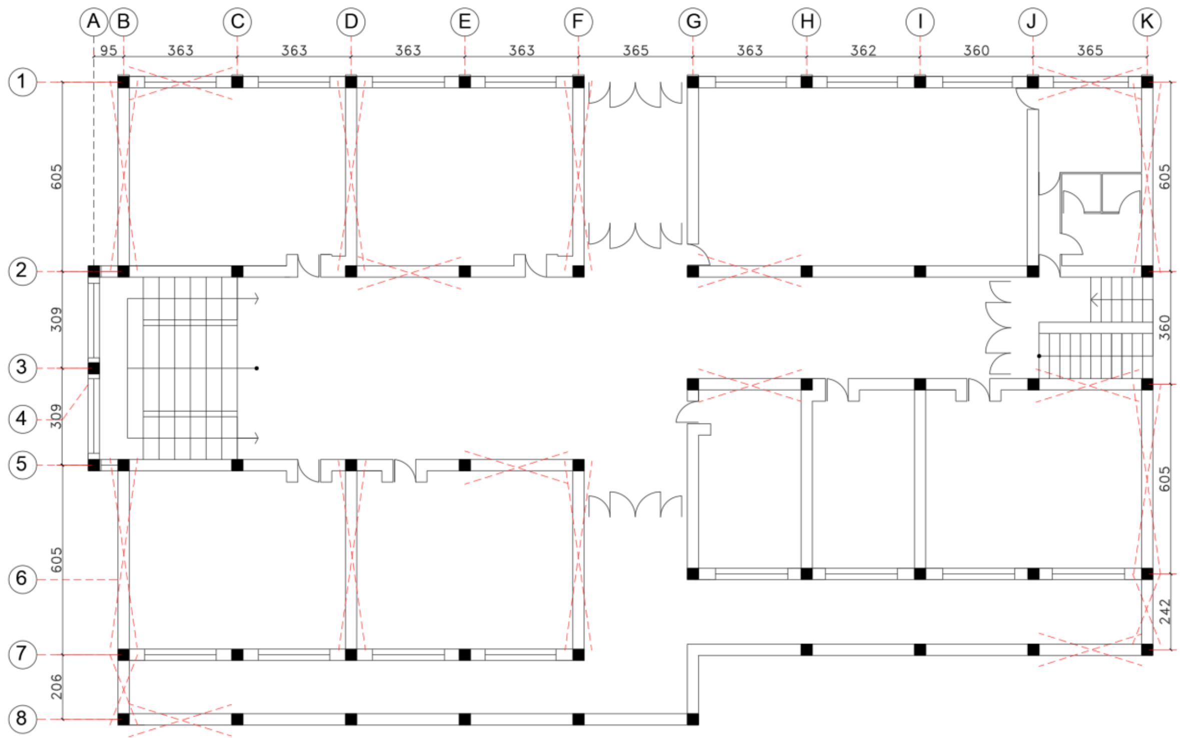

(c)

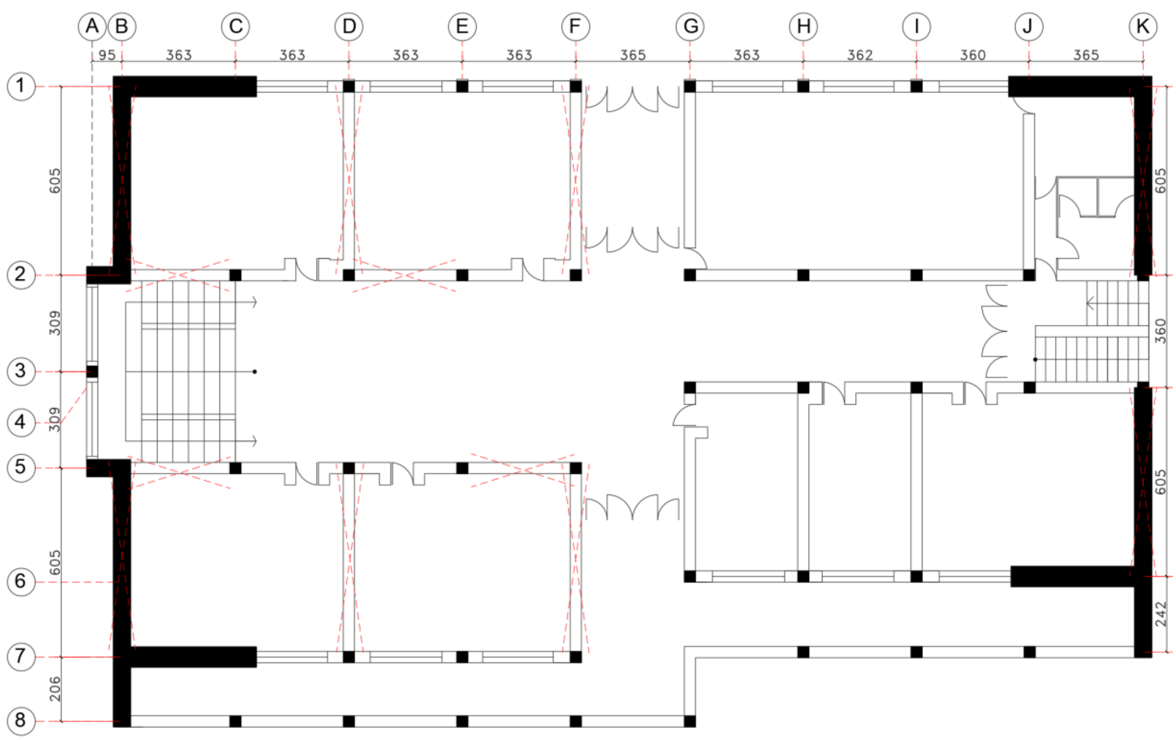

(d)

Fig. 2. Case study: (a) view of the existing school; (b) plan view of the existing school; (c) plan view of the retrofitting option with concentric braces; (d) plan view of the retrofitting option with RC shear walls.

The sections of beams include IPE140, IPE160, IPE200, UNP240, and CPE200. The plan of the beams of the floors is presented in **Appendix A**. The sections of the school's columns include 2IPE160, IPE200+INP200, 2UNP160, 2IPE200, and 2UNP180 and there is no change in the column section in the height of the school. The section of all existing braces in all stories is UNP65.

The destructive and non-destructive tests on the school columns, beams, braces, etc. were conducted to determine the properties of the materials in the structure. Based on the results of these tests, the separating and surrounding walls in this school are made of compressed bricks and due to their shear resistance, they are considered as masonry infill walls. These masonry infill walls with thicknesses of 10, 22, and 35 cm have been used in this school.

Table. 1 presents the expected and lower bound strength of materials in this school which have been obtained based on experimental tests.

Table. 1. Lower bound and expected strength of materials (kg/cm^2).

Strength Case	Steel Yielding Strength for Columns, Beams, and Braces
Expected strength	3000
Lower bound strength	2400

In 2012, based on the request of DRES, the vulnerability assessment of the existing school was carried out by consulting engineers. In order to achieve the vulnerability assessment, nonlinear static analysis (Pushover) has been done. Then, different schemes for retrofitting the existing school were obtained. The parameters of **Table. 2** are used in the nonlinear analysis of the existing school.

Table. 2. Parameters for nonlinear analysis of the existing school.

Design Parameter	Value
Dead load of stories	6.061 KN/m^2
Dead load of roof	7.708 KN/m^2
Live load of stories	1.961 KN/m^2
Live load of roof	1.471 KN/m^2
Gravity load	1.1 (Q_D+Q_L)[a] and 0.9(Q_D)

[a] Q_D=Dead load & Q_L=Live load.

The following assumptions are considered in the nonlinear analysis of the existing school:

- The Iranian instruction for seismic rehabilitation of existing buildings (code No.360) has been used to present different schemes for retrofitting the school. Based on this instruction, The gravity load (Q_G) was combined with the seismic load (Q_E) as follows:

$Q_{UD} = Q_G \pm Q_E$

- The interaction between the soil and the structure is ignored in the analysis, but the P-Delta effects are considered.

The results of the analysis show that the main reason observed in the structural system of this school building is the weakness of the lateral bearing system. Also, the inappropriateness of the sections used in the concentric braces and an insufficient number of them are other defects in the structural members of this building. As a result, the building is currently less able to withstand the lateral loads caused by the earthquake and will be vulnerable in this regard. FEMA-547 [59] suggests two options for providing lateral strength and stiffness of structures:

1. Adding lateral bearing systems to existing structure.
2. Retrofitting of existing elements of structure.

Option 2 is ignored due to the large amount of destruction of the existing school elements and the time-consuming process of retrofitting of existing elements of the school.

Finally, two retrofitting options including retrofitting with concentric braces and retrofitting with shear walls have been proposed, which are presented in **Figs. 2(c)** and **(d)**, respectively. In retrofitting option with concentric braces, the section of all existing braces is changed to new sections according to **Table. 3**. Also, in retrofitting option with shear walls, according to **Fig. 3**, a wall with a thickness of 30 cm in the x direction and 40 cm in the y direction with two plates of longitudinal and transversal reinforcements is considered as a lateral load-bearing system. The concrete of the shear wall has a strength of $f'c=250$ kg/cm^2 while the rebars have a yield strength of $fy=4000$ kg/cm^2.

Table. 3. The brace sections in both x and y directions of retrofitting option with concentric braces.

Story	Brace Section
1	2UNP140
2	2UNP100
3	2UNP80

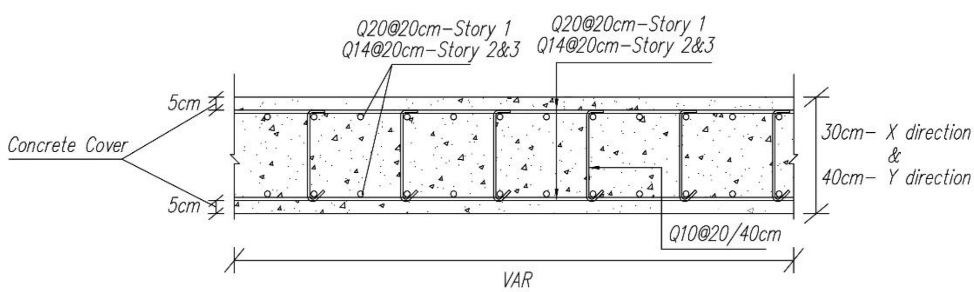

Fig. 3. Section of shear wall

From the two retrofitting options of the existing school, due to the following reasons the retrofitting option with shear walls was chosen as the final option of retrofitting by the consulting engineers.

- Significant reduction of lateral displacements due to a significant increase in the stiffness of the structure.
- Eliminating the issue of strengthening the sections of beams and columns due to the absorption of a large percentage of earthquake shear by shear walls.
- The ability to perform most of the retrofitting operations outside the building and as a result, less impact on the internal components and elements of the school.
- Removing the issue of strengthening the connection between elements in this school.
- Faster implementation than retrofitting option with concentric braces.
- Based on the financial estimate made by the consulting engineers, this option has lower financial costs compared to the other option.

In this study, as mentioned above, the appropriate retrofitting option for the existing school is determined based on the resilience index with FEMA P-58 methodology.

4. Modelling and analysis

4.1. Modeling in OpenSees

To perform IDA with the "Hunt-Fill" algorithm, OpenSees software is used. This software is a complete collection of all kinds of elements, materials, and different methods of analysis. So the existing school building and its retrofitting options are modeled in OpenSees. Due to the regularity of the structure in the plan and elevation, a two-dimensional model has been used for modeling. Therefore, the assessment of frame K in the N-S direction only is presented in the research reported in this paper. In this research, sections are modeled by fiber elements. Beams, columns, braces, and reinforcements used in shear walls have been modeled by Steel02 materials in the OpenSees library, while Concrete01 material was used to model shear walls in the software. The "forceBeamColumn" element is used to model the beams and columns. All models include a column (gravity-leaning column) with no lateral stiffness to simulate P-Delta effects associated with gravity loads on the lateral bearing frames. The modeling of braces in this research is based on the method presented by Gunnarsson in previous studies (Gunnarsson 2004). In this study, the buckling behavior of the brace is simulated by 10 forceBeamColumn elements along the length of the brace (**Fig. 4**). To predict brace buckling an initial displaced shape is considered by a sinusoidal function with an amplitude equal to 1/1000 of the length of the brace. For more information on the details of modeling the buckling behavior of braces, readers are referred to Gunnarsson (2004).

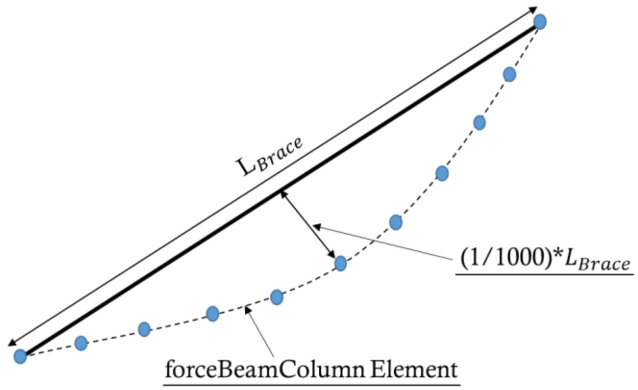

Fig. 4. Modeling the buckling behavior of braces in OpenSees software.

After modeling the existing school building in OpenSees software, the fundamental period of the structure is compared in OpenSees with one in ETABS 2016 V16.2.1. The comparison between the period of the structure in OpenSees, 0.7231 sec, with that in ETABS, 0.7118 sec, indicates the accuracy of modeling.

The model of the first rehabilitation option, with concentric braces, is the same as the existing structural model, except that the bracing sections and the number of braced bayes are increased. Comparing the period of the first mode of the structure in OpenSees (T_1= 0.4185 s) and ETABS (T_1= 0.4174 s) software and the proximity of these two values confirms the accuracy of the constructed model.

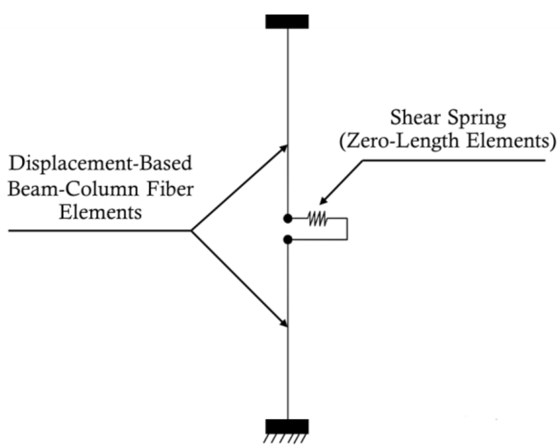

Fig. 5. Model discretization of the shear wall system.

In this study, the equivalent column method has been used to model the shear wall. In this way, the concrete shear wall is represented by a column with a cross-section equivalent to the shear wall placed at the center of the wall surface and connected to the surrounding beams at the floor level by rigid elements (Samadian et al. 2019). Displacement-based beam-column elements have been used to model the shear wall, but as the behavior of the shear walls in this study is controlled by shear, these elements are not capable of capturing shear deformation alone (Hosseinzadeh and Galal 2020b). So, the dispBeamColumn element is used to model the equivalent column, and on each floor, a translational shear spring is modeled by the zeroLength element in the middle of the floor height. The model discretization of the shear wall system is presented in **Fig. 5**. More information about the modeling of shear walls and considered parameters are provided by Gogus (2010) and Gogus and Wallace (2015).

4.2. Ground motion selection and seismic analysis

In this study, to consider mainshock-aftershock sequences, the effect of mainshock damage on the structure before applying the aftershocks has been evaluated (Li et al. 2014). There are three performance states for buildings, including Immediate Occupancy (IO), Life Safety (LS), and Collapse Prevention (CP) according to ASCE41. These three performance states are defined by 0.007, 0.025, and 0.05 maximum inter-story drifts for steel buildings. The three performance states can be viewed as minor, moderate, and severe damage to the steel frame. So, in this study, to indicate the mainshock damage on the structure before applying the aftershocks, the response levels 0.007, 0.025, and 0.05 maximum inter-story drift values have been considered (Li et al. 2014); (Jalali et al. 2021).

The following steps were taken to investigate the effects of mainshock-aftershock sequences in this study:

- First, an IDA using the mainshock records is performed with the Hunt-Fill method. By performing IDA, a response-intensity relationship is obtained for each mainshock record.
- In this study, to indicate the mainshock damage, the response levels 0.007, 0.025, and 0.05 maximum inter-story drift values have been considered. The intensity corresponding to each response level is interpolated from the intensity response relationship of the previous step. Then, another IDA is performed using the mainshock scaled to the intensity corresponding to a specific damage level.
- After performing an IDA for each mainshock record in the previous step, in order to have the structure in the residual stage, a free-vibration analysis is considered (for more information about free-vibration analysis, refer to the paper presented by Jalali et al. 2021).
- Eventually, an IDA using the aftershock records is performed with the Hunt-Fill method. In IDA using aftershock records, the aftershock scaling process is such that the intensities increase incrementally until the structure collapses.

Fig. 6 provides a schematic flowchart to explain the scaling of the mainshock-aftershock event.

In this study, 32 mainshock-aftershock (MS-AS) seismic sequences recorded from the Center for Engineering Strong Motion Data (CESMD) and the Pacific Earthquake Engineering Research Center (PEER NGA [60]) explained by (Han et al. 2014) were used for IDA. Most of the selected aftershocks occurred within a week after the mainshock, so there was not enough time to repair the structure before the aftershock. The moment magnitude (M_m) of mainshocks and aftershocks varies from 5.8-7.2 and 5.0-6.7, respectively. The average shear wave velocity in the upper 30 meters (V_{S30}) of each station is generally between 183 m/s to 367 m/s, which indicates that their site conditions are consistent with the site conditions of the school building in this study (soil type III according to standard NO.2800). The characteristics of the selected records are presented in **Table B1.** Appendix.

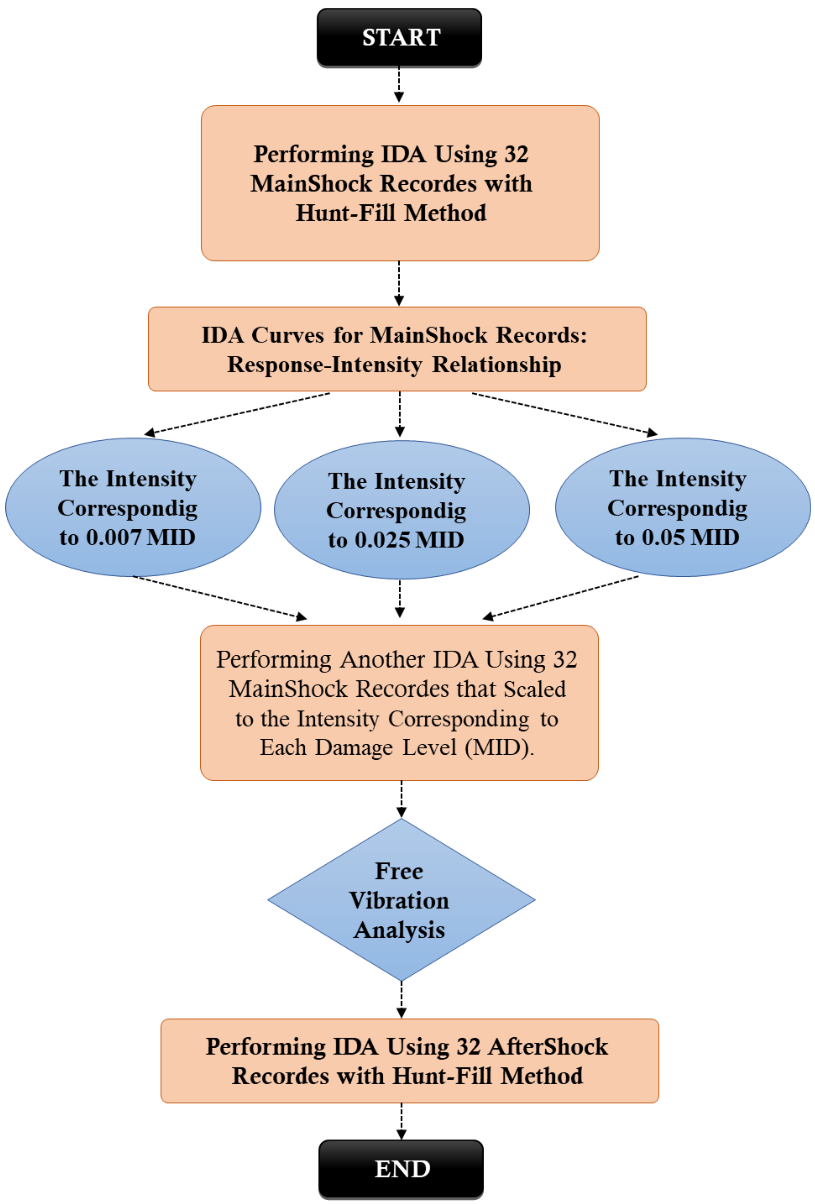

Fig. 6. A schematic flowchart to explain the scaling of the mainshock-aftershock event

The results of IDA under the mainshock records for the existing school building and its two retrofitting options are shown in **Fig. 7**, and to compare the IDA curves of the existing school and its retrofitting options, their median IDA curves are presented in **Fig. 7(d)**. It is important to note that in this study, the median IDA curve is presented only for easier and clearer comparison of the results of the IDA curves, and the output of the IDA curves of all 32 mainshock records as well as mainshock-aftershock sequences are used for further investigation such as resiliency. In IDA curves, the horizontal axis represents the maximum inter-story drift ratio, which is considered as the Engineering Demand Parameter (EDP), and the vertical axis represents pseudo acceleration in a fundamental period of structure with damping of 5%, which is selected as an intensity measure parameter.

As shown in **Fig. 7(d)**, retrofitted structures compared to the existing school experience a certain maximum inter-story drift ratio in greater intensities. Therefore, the retrofitting operation has improved the seismic performance of the school structure.

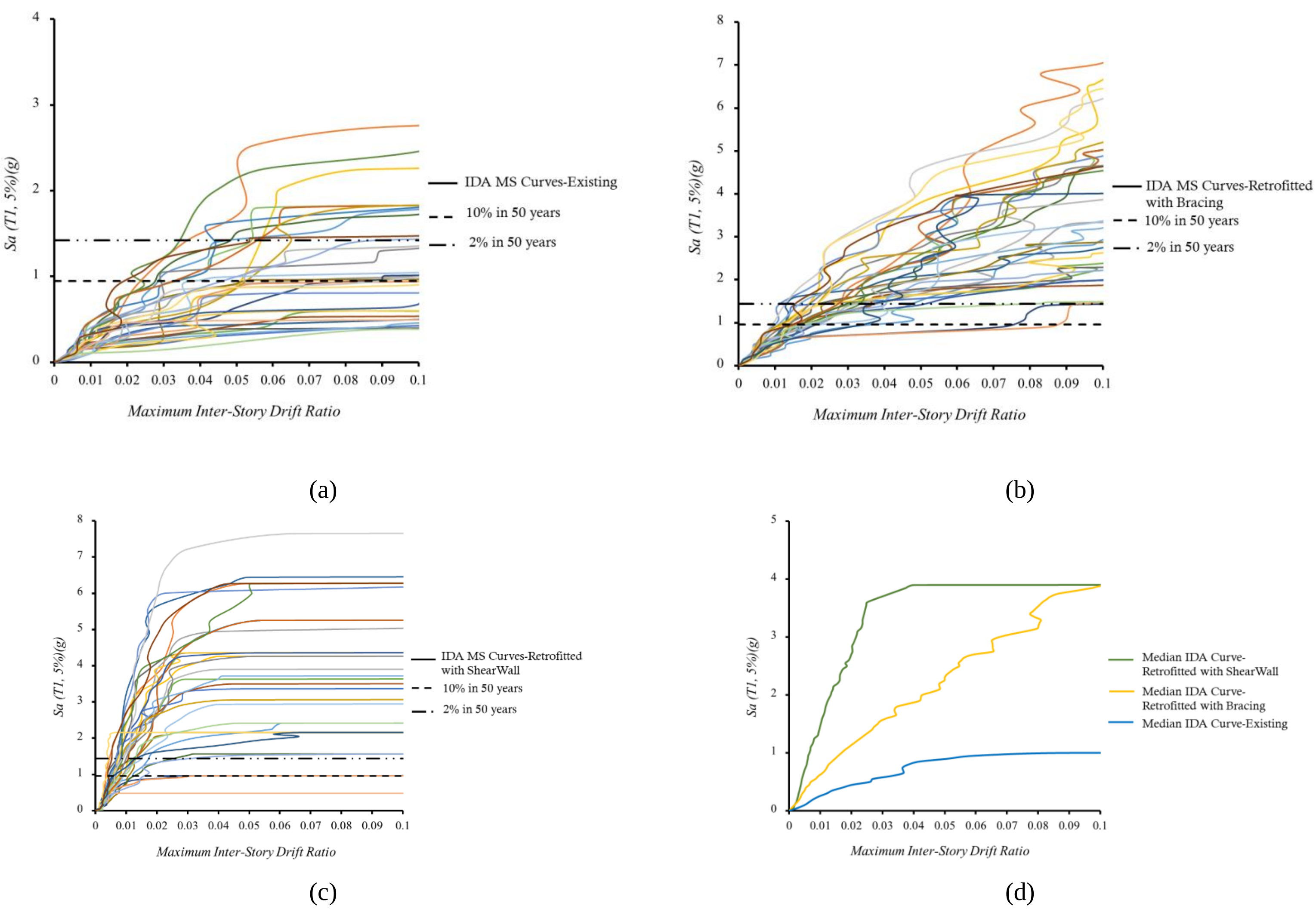

Fig. 7. Mainshock IDA curves: (a) for existing school; (b) for retrofitted with bracing; (c) for retrofitted with shear walls; (d) median IDA curves for three types of schools.

The results of IDA under the aftershock records following the mainshocks are shown in **Fig. 8** for the existing school and its retrofitting options. As shown in **Fig. 8**, a horizontal lag occurs at the beginning of the IDA curves of the structures under the effect of different scenarios of mainshock-aftershock due to the maximum inter-story drift response that is created at the end of the mainshock in the structure. As the damage of the mainshock increases, the value of this horizontal lag at the beginning of the IDA curves becomes larger.

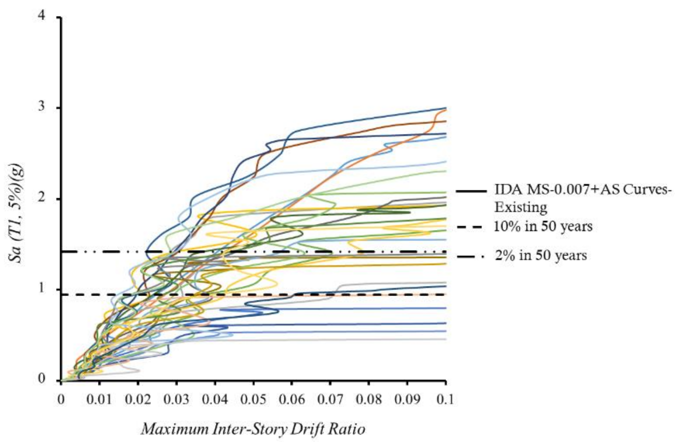

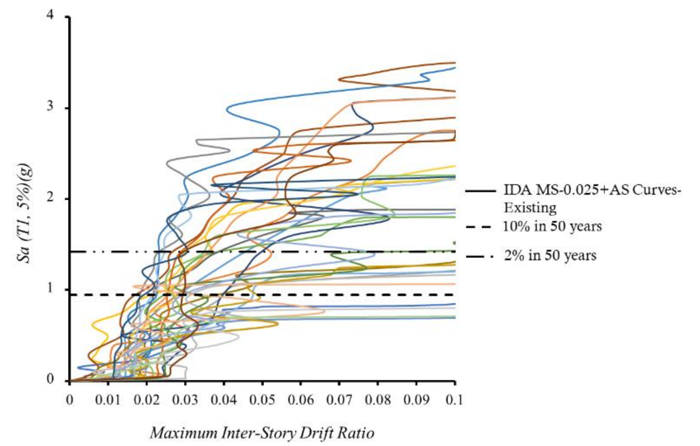

(a)

(b)

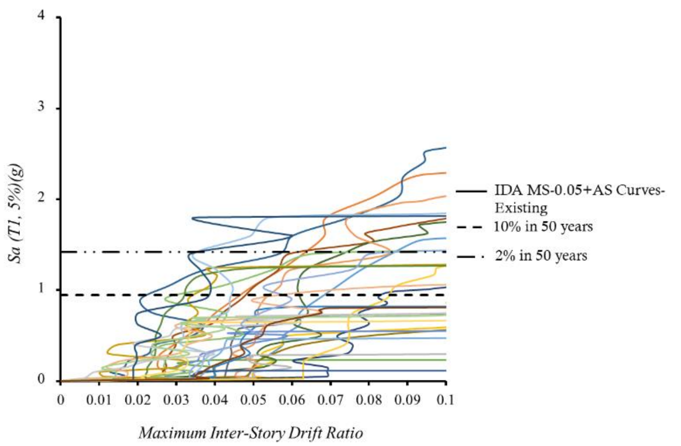

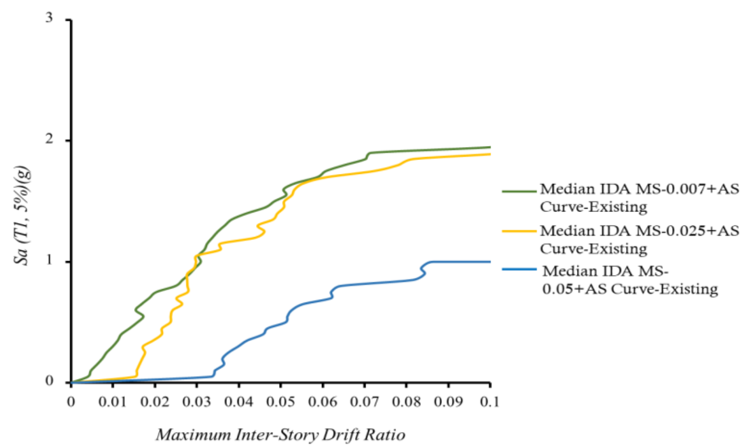

(c)

(d)

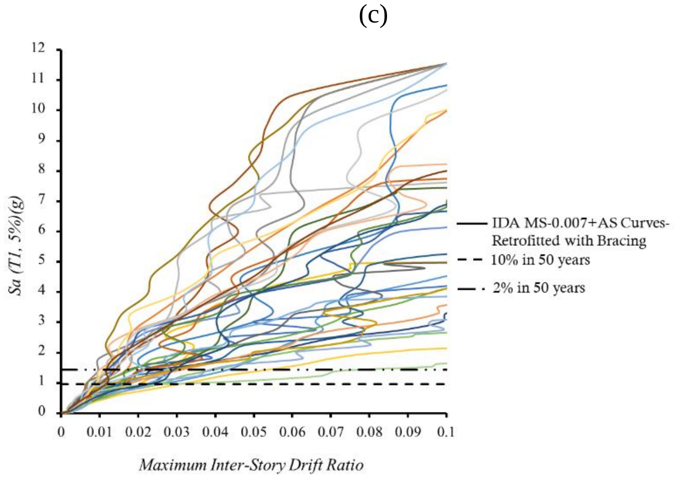

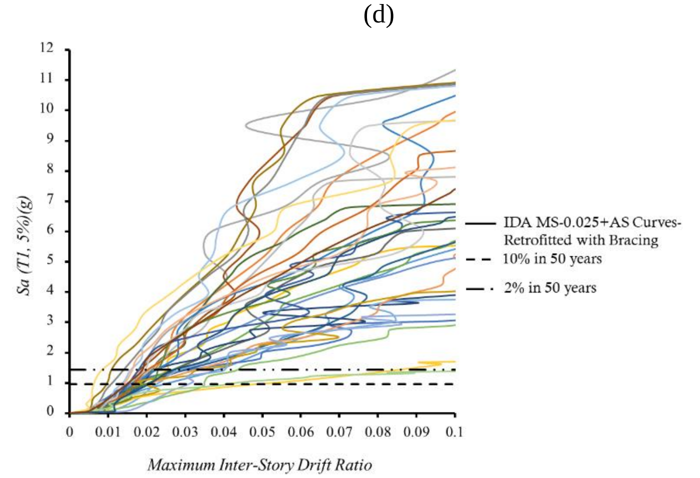

(e) (f)

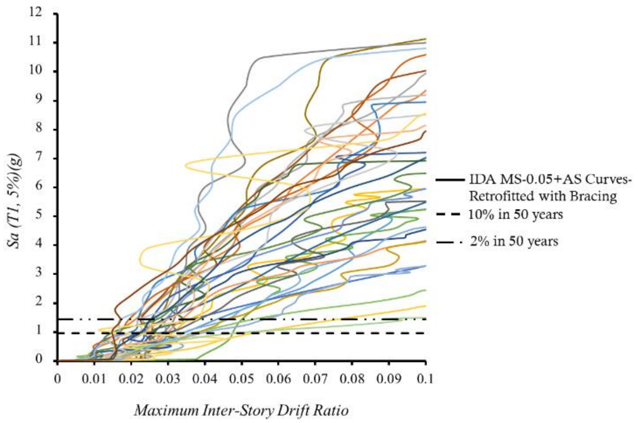

(g)

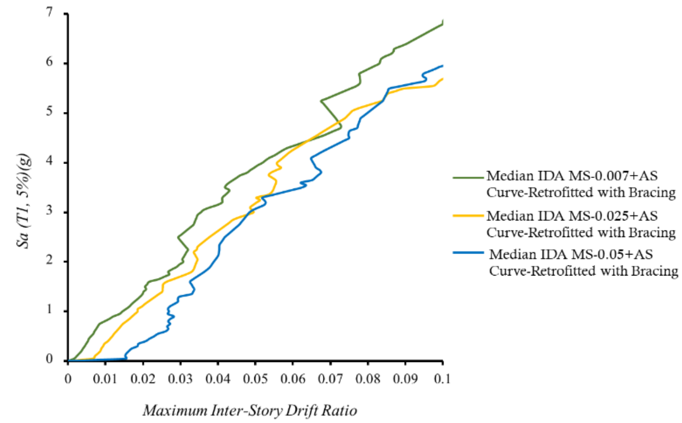

(h)

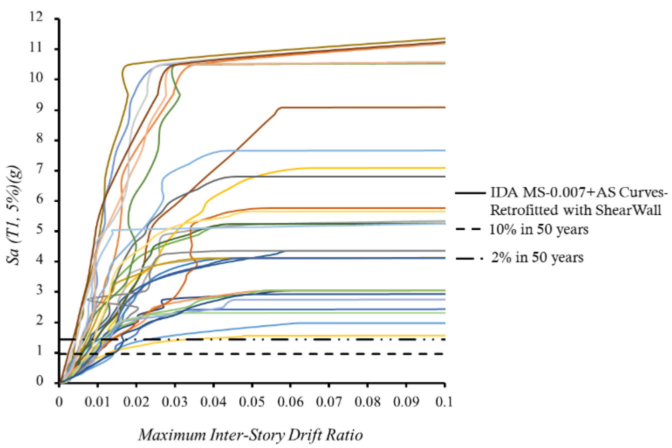

(i)

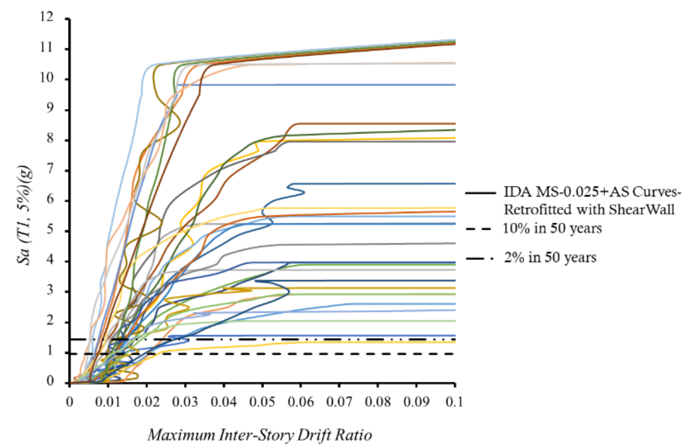

(j)

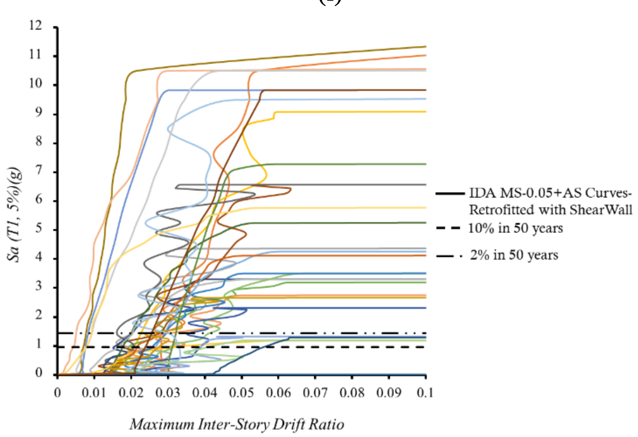

(k)

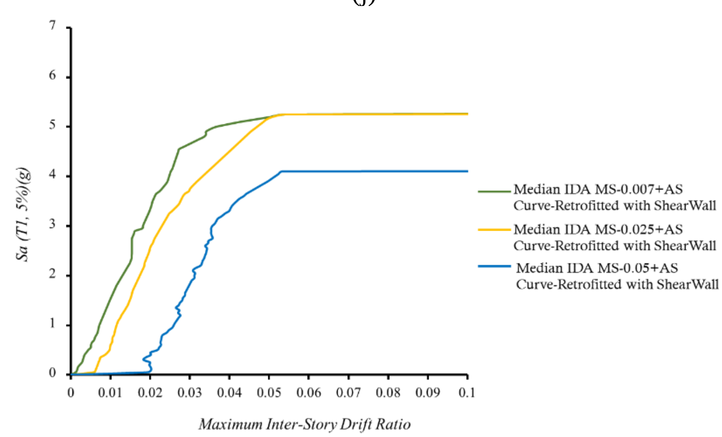

(l)

Fig. 8. IDA curves for three types of schools under different scenarios of the MS-AS application.

To compare the IDA curves of the structures under different scenarios of the mainshock-aftershock application, the median values of the IDA curves are shown in **Figs. 8(d), (h),** and **(l)**. According to median IDA curves, if the level of damage caused by the mainshock increases, the collapse capacity of the structure will decrease under the effect of the aftershock. The median IDA curves corresponding to the damage levels of 0.007 and 0.025 are not significantly different from each other, but by increasing the mainshock MID level to 0.05, a relatively significant difference is observed in the median IDA curve, especially in the existing school.

4.3. Seismic damage assessment

In this section, the damage assessment process based on FEMA P-58 methodology is presented. After performing IDA and considering the effects of different scenarios of the MS-AS, the results obtained in the previous step are used to assess the seismic damage of the existing school and its retrofitting options. The seismic performance of any type of building, regardless of age, construction method, or type of occupancy, can be evaluated with the method provided by FEMA P-58 (FEMA P-58-2). PACT is developed as a calculation tool of FEMA P-58 methodology to estimate repair cost and time required to restore the structure to its pre-earthquake condition. The modeling process in PACT software is done in three steps. In the first step, the basic information about the building, including its total replacement cost, replacement time, occupancy type, story height, and floor area should be introduced to the software. It should be noted that PACT calculates the cost of repairs based on the year 2011 in Northern California, so by using a multiplier, the costs can be evaluated based on the desired year and the location of the case study. **Table. 4** includes the total replacement cost of the existing school and its retrofitting options in Iran, the replacement time of all three schools, and the occupancy type of structures. In **Table. 4**, the building cost of a typical school in Iran has been converted from Rial currency to U.S. dollars, and these costs have been calculated based on the cost of construction in Iran. For example, the replacement cost of the existing school is $250 per square meter (DRES 2020). Considering that the area of the school is 1,920 m^2, the total replacement cost is $480,000. After defining the general characteristics of the building in PACT, in the next step, the fragility curves related to the structural and non-structural components of the building should be selected from the PACT library, which is based on FEMA P-58 methodology. Subsequently, the quantity of each component must be assigned. The components selected from the PACT library and their quantities are presented in **Table. C1** Appendix.

Finally, the EDPs obtained by the seismic analysis of the structure in OpenSees are entered into PACT for each hazard level. The Monte Carlo method is used by PACT for a large number of realizations. In this case, random numbers and fragility curves are used to determine whether the specific components are damaged. Regarding the determined damage state, the repair cost and repair time are obtained. PACT sums the repair costs and repair time of all components of the structure for each realization, and in this way, the cumulative distribution function for repair cost and repair time is obtained. The median value of this function is used as the repair cost and time of structure.

Table. 4. The basic information of the buildings.

Type of Building	Total Replacement Cost ($)	Replacement Time (Day)	Occupancy Type
Existing School	480,000	365	Education (k-12): High Schools
Retrofitted with Bracing	620,000	365	Education (k-12): High Schools
Retrofitted with ShearWall	595,200	365	Education (k-12): High Schools

As mentioned, the seismic damage assessment of schools in this study is done for two hazard levels including 10% and 2% in 50 years. The repair cost and repair time of the existing school building and its two retrofitting options, when they are under the effect of the mainshock, are extracted by PACT as presented in **Fig. 9** and **Table. 5**.

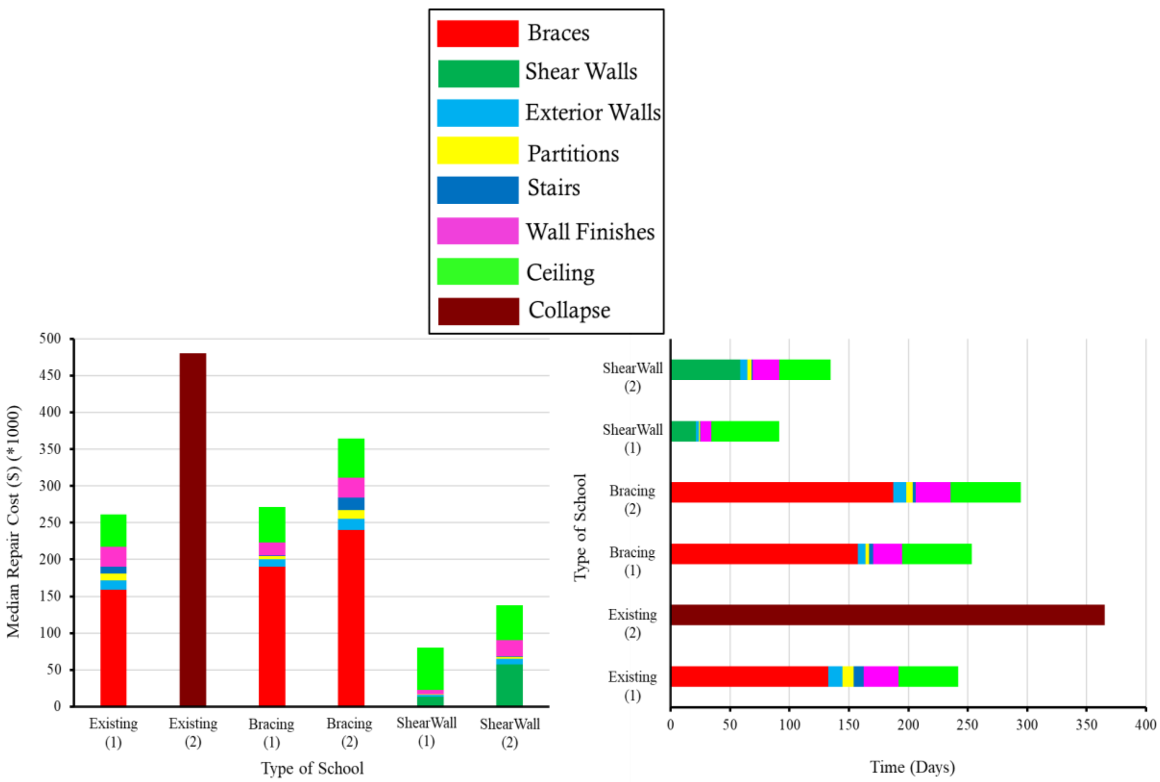

(a) (b)

Fig. 9. Damage assessment for three schools for two hazard levels (1&2) under the effect of the mainshock: (a) Repair Cost; (b) Repair Time

As shown in **Fig. 9(a)**, the total repair cost at the second hazard level (2% in 50 years) is greater than that at the first hazard level (10% in 50 years) for all three structures. In this study, the loss is considered based on dividing the total repair cost by the total replacement cost. The existing school has completely collapsed at hazard level 2 and has a 100% Loss. When the structure collapses, PACT does not provide any information related to the damage to the components of the structure and only shows the repair cost/time equal to the replacement cost/time of the structure, so the repair cost and repair time of the existing school at hazard level two due to the collapse, is equal to the replacement cost and replacement time according to **Fig. 9**. The braces of the existing school have the most repair cost compared to other components, and this issue is consistent with the content of Section 3. Also, it can be seen that from the total repair time of the existing school, which is approximately 242 days, the most repair time is allocated to the repair of braces, which includes 132 days. The concentric braces of the retrofitted option in both hazard levels have the most repair cost and repair time than the other components of the school and because the number of braces in this option is more than the braces of the existing school, their repair cost and repair time are greater than the braces of existing school. According to this bar chart (**Fig. 9(a)**), the structural components of a retrofitted school with shear walls have suffered less damage than those of the existing school and retrofitted school with bracing. Therefore, this option has a lower repair cost and damage than the other two schools in both hazard levels. Also, it can be seen that the ceiling, which is a non-structural component and is sensitive to acceleration, has a larger repair cost and time than other non-structural components in all three structures.

Table. 5. The total repair cost and repair time of the existing school and its retrofitting options under the effect of the mainshock.

Type of Building	Seismic Hazard Level	Total Repair Cost ($)	Total Repair Time (Day)	Loss (%)
Existing School	1	261,489	241.86	54.48
	2	480,000	365	100
Retrofitted with Bracing	1	270,967	253.24	43.70
	2	364,663	294.48	58.82
Retrofitted with ShearWall	1	80,580	91.13	13.54
	2	137,580	134.38	23.11

The data in **Table. 5** shows the total repair cost, repair time, and loss of the existing school and its retrofitting options according to **Fig. 9**. The third column of the **Table. 5** shows the total repair cost of the buildings under the effects of the mainshock, where the loss of each building is obtained by dividing the total repair cost by the total replacement cost (**Table. 4**). For example, for an existing school in hazard level 1, the total repair cost is $261,489 and the total replacement cost is $480,000. So, the loss of existing school at hazard level 1 (54.48%) is obtained by dividing these two values.

After evaluating the seismic damage of all three schools under the effects of the mainshock, the repair cost and repair time of these structures are extracted from PACT under different scenarios of the mainshock-aftershock. The results are presented in **Fig. 10**, **Tables. 6, 7,** and **8**.

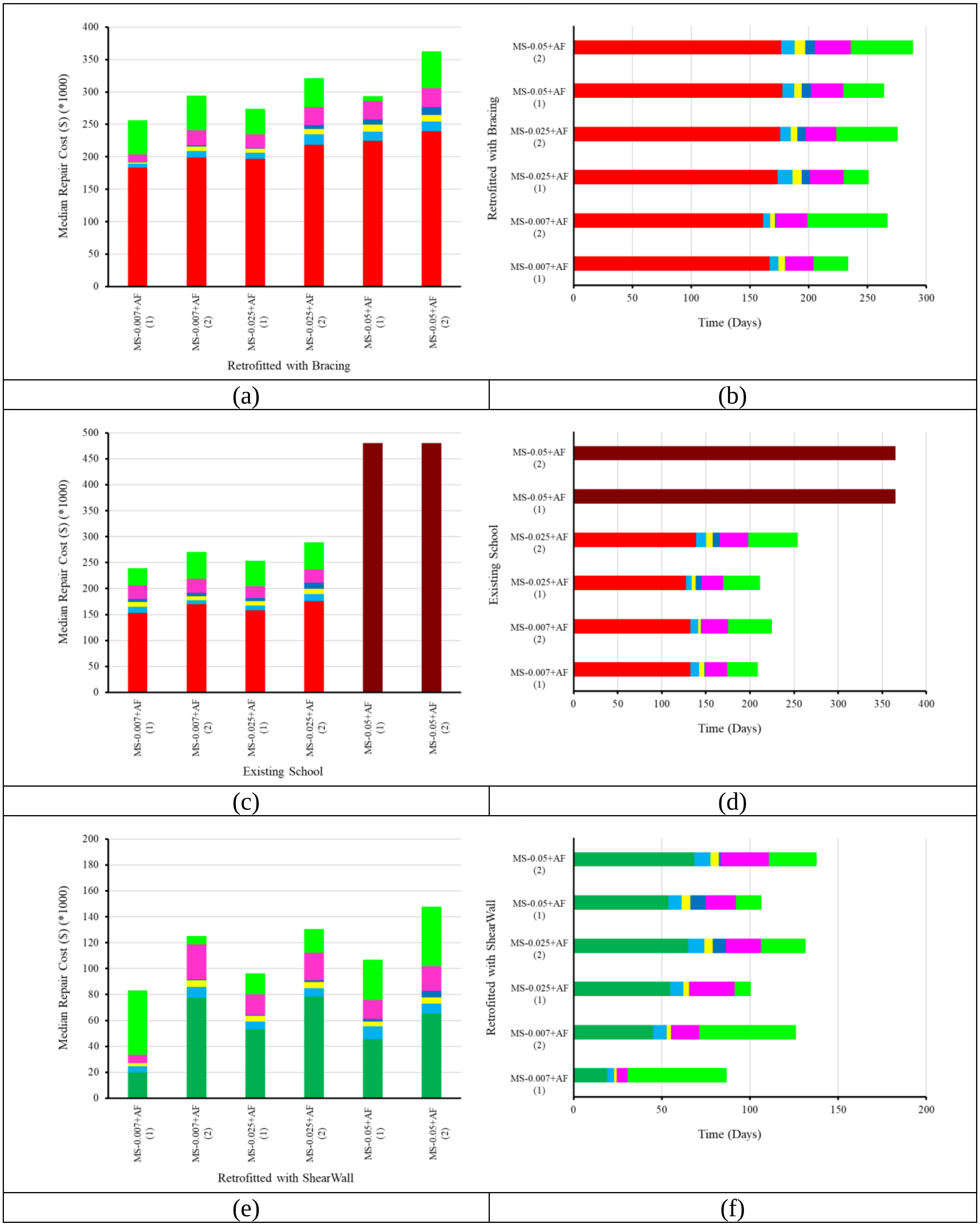

Fig. 10. Damage assessment for three schools for two hazard levels (1&2) under different scenarios of the MS-AS.

Table. 6. The total repair cost and repair time of the existing school under different scenarios of the MS-AS.

Senario of MainShock-AfterShock	Seismic Hazard Level	Total Repair Cost ($)	Total Repair Time (Day)	Loss (%)
MS-0.007+AS	1	239,176	208.71	49.83
	2	270,634	224.67	56.38
MS-0.025+AS	1	253,808	211.24	52.88
	2	289,000	254.33	60.21
MS-0.05+AS	1	480,000	365	100
	2	480,000	365	100

Table. 7. The total repair cost and repair time of the retrofitted school with concentric braces under different scenarios of the MS-AS.

Senario of MainShock-AfterShock	Seismic Hazard Level	Total Repair Cost ($)	Total Repair Time (Day)	Loss (%)
MS-0.007+AS	1	256,220	233.48	41.33
	2	293,977	266.91	47.42
MS-0.025+AS	1	274,170	251.08	44.22
	2	321,429	275.67	51.84
MS-0.05+AS	1	293,353	263.90	47.32
	2	362,700	288.67	58.50

Table. 8. The total repair cost and repair time of the retrofitted school with shear walls under different scenarios of the MS-AS.

Senario of MainShock-AfterShock	Seismic Hazard Level	Total Repair Cost ($)	Total Repair Time (Day)	Loss (%)
MS-0.007+AS	1	83,308	86.72	14.00
	2	124,976	126.20	21.00
MS-0.025+AS	1	96,246	100.53	16.17
	2	130,514	131.50	21.93
MS-0.05+AS	1	106,900	106.57	17.96
	2	147,954	137.71	24.86

According to **Figs. 10(a)** and **(b)** which show the repair time and repair cost of the existing school under the effect of different scenarios of MS-AS, the existing school has collapsed under the effect of a 0.05 damage level of the mainshock in both hazard levels and has 100% loss. Also, the time required for its repair is equal to the replacement time. As explained in Section 3, the existing school has a weak lateral resisting system, so by increasing the mainshock MID level to 0.05, the structure is significantly damaged after applying the aftershock but the amount of damage to the existing school under the effect of the other two scenarios is not significantly different from each other.

The data in **Table. 6, 7, and 8** show the total repair cost, repair time, and loss of the existing school and its retrofitting options according to **Fig. 10**. The third column of all **Tables** shows the total repair cost of the buildings under different scenarios of the MS-AS, where the loss of each building is obtained by dividing the total repair cost by the total replacement cost (**Table. 1**).

As shown in **Tables. 7, 8,** and **Fig. 10**, by increasing the mainshock MID level, the initial damage caused by the mainshock leads to insignificant changes in the amount of repair cost/time of the retrofitted schools under the different scenarios of MS-AS. For example, by increasing the mainshock MID level to 0.05 in the retrofitted school with concentric braces, the amount of loss at hazard level one has reached from 41.33% to 47.32% (About a 4% increase).

4.4. Calculation of the delay time in starting the recovery process

In this study, the delay time between the earthquake event and the beginning of the recovery process is calculated by two methods. One of these methods is based on the DRES database and the other is according to REDi guideline.

According to the information obtained from the DRES database, if the damage to the structure exceeds 35%, the delay time in starting the recovery operation is considered to be 365 days, and this means that the retrofitting operation is not economically acceptable and the structure must be reconstructed and for damages less than 35%, a linear interpolation is performed and the delay time is calculated (Samadian et al. 2019). The delay time based on the DRES database for the existing school building and its retrofitting options is presented in **Table. 9**.

The REDi guideline calculates the repair time of the damaged components based on the data extracted from the PACT more accurately and also estimates the delay time at the beginning of the recovery process. REDi guidelines consider these delays as "impeding factors" because these factors prevent the start of the recovery process. These impeding factors include the inspection of the structure after the earthquake event, gathering experts to determine the type of recovery operations (rehabilitation or reconstruction), financial resources for repairs, assigning contractors, obtaining permits related to repairs/reconstruction, and the provision of "long-lead time" components by the contractor (Almufti and Willford, 2013). Three Repair Classes (RC) are defined in the REDi guideline, which includes Class 1 with minor structural damage, Class 2 with damaged non-structural components, and Class 3 with severely damaged structural and non-structural components. Impeding factors are calculated based on impeding curves in the REDi guideline (**Table. 10**). According to REDi, some of these delays occur simultaneously, so the total delay time is obtained from the combination of these impeding factors (the combination of delay times calculated in **Table. 10**) (refer to Almufti and Willford (2013)). The total delay time for the existing school, retrofitting options with concentric braces and shear walls (after a combination of delay times are in **Table. 10** according to REDi guideline) are 406, 406, and 161 days, respectively.

Table. 9. The delay time based on the DRES database.

MainShock/ MainShok-AfterShock	Seismic Hazard Level	Delay Time (Day)		
		Existing School	Retrofitted with Bracing	Retrofitted with Shear Walls
MainShock	1	365	365	141
	2	365	365	241
MS-0.007+AS	1	365	365	146
	2	365	365	219
MS-0.025+AS	1	365	365	365
	2	365	365	365
MS-0.05+AS	1	365	168.63	187
	2	365	228.7	259

Table. 10. Impeding Factors based on the REDi guideline.

Impeding Factor	Type of School		
	Existing	Retrofitted with Bracing	Retrofitted with Shear Walls
Post-Earthquake Inspection	5 days	5 days	-
Gathering Engineers	50 weeks	50 weeks	12 weeks
Financing	-	-	-
Gathering Contractors	23 weeks	23 weeks	23 weeks
Permitting	8 weeks	8 weeks	8 weeks

* It is assumed that financial resources are available to repair the school structure, so there will be no delay time in this regard.

It can be seen that in calculating the delay time using the Redi guideline, various factors are considered as obstacles to initiating the recovery process which are not considered in the information obtained from the DRES database. This leads to a more accurate calculation compared to the DRES method. Therefore, the calculated delay time using REDi guideline has been used in assessing the resilience index of schools.

5. Functionality curve and seismic resilience index

Since the purpose of this study is to select the appropriate retrofitting option for a steel school building according to the seismic resilience index, in this section by obtaining the functionality curves of schools and calculating the resilience index, the appropriate retrofitting option can be determined.

Based on the definition of resilience (Cimellaro et al. 2010), "Resilience is defined as a function (functionality curve) that indicates the capacity to maintain the level of performance of a certain building over a period of time (control time)", in this study, for resilience comparison between all schools, the same control time should be adopted. Hence, the control time for all three schools is considered to be 771 days, which is obtained by adding the maximum delay time at the beginning of the recovery process (406 days) to the maximum repair time (365 days). The total damage to schools after the earthquake event, the repair time, and the delay time at the beginning of the recovery process are the necessary data to evaluate the functionality curves that are obtained in the previous sections. The resilience index of the existing school and its retrofitting options at both hazard levels under the effect of the mainshock are presented in **Fig. 11** and **Table. 11**, respectively.

In this study, it is assumed that the performance of the structure was 100% before the earthquake event, and after the recovery operation, its performance will reach 100% again. According to **Fig. 11**, the beginning of the functionality curve is a value smaller than 1, which indicates the damage (loss) caused by the seismic event, and in all curves, after passing the delay time and the recovery process, the performance of the structure becomes 100%. It can be concluded that the functionality curves of both retrofitting options at the first hazard level are above the curve of the existing school and the functionality curves of all three schools at the second hazard level are below the curves of hazard level one (the curves shown by dashed lines in **Fig. 11**), and also all three schools have a smaller resilience index at the hazard level 2.

The existing school at the second hazard level has completely collapsed and according to the data extracted from the PACT, the damage of this school is 100% and the repair time is 365 days, so its functionality curve has started from zero, and after 771 days, the recovery process has been completed and the performance of the school reaches 100%. It can be seen that the area under the functionality curve of the existing school at hazard level 2 is equal to zero, with a zero resilience index. By evaluating the seismic damage of the retrofitted school with shear walls in the previous sections of this study, it was found that this option has less repair cost, repair time, and delay time. So, the area under its functionality curves is greater compared to the area under the functionality curves of the other two structures and according to **Table. 11**, it has greater resilience indexes than the other two schools in both hazard levels. Thus, the performance of this retrofitting option against the seismic event is better than another option.

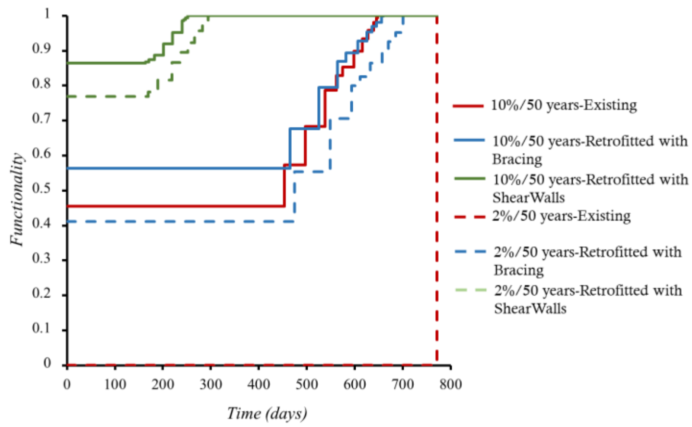

Fig. 11. Functionality curves for the existing school and two retrofitting options under the effect of the mainshock

Table. 11. Seismic resilience index for the existing school and two retrofitting options under the effect of the mainshock.

Seismic Hazard Level	Resilience Index		
	Existing School	Retrofitted with Bracing	Retrofitted with ShearWalls
1	0.6206	0.6916	0.9620
2	0	0.5604	0.9287

In this study, it is concluded that by retrofitting the existing school, the resilience index at hazard level one will increase from 0.6206 to 0.6916 and 0.9620 in retrofitting options with concentric braces and shear walls, respectively, and also it will improve from 0 to 0.5604 and 0.9287 at the second hazard level, indicating the improvement of the seismic performance of the structures as a result of retrofitting. A comparison between the resilience index of the existing school and its retrofitting options is shown in **Fig. 12**.

The functionality curves and resilience index of the existing school and its retrofitting options under different scenarios of mainshock-aftershock are presented in **Fig. 13** and **Table. 12,** respectively.

Based on the data extracted from PACT, the existing school has completely collapsed in both hazard levels under the effect of 0.05 damage level of the mainshock, and as shown in **Fig. 13(a)**, its functionality curve started from zero and after the recovery process, it reached the pre-earthquake condition. Also, the damage assessment of retrofitted school with concentric braces indicates that its structural components have been severely damaged under the effect of the mainshock and different scenarios of mainshock-aftershock, so the area under its functionality curves is smaller than the other option and as a result, it has a smaller resilience index.

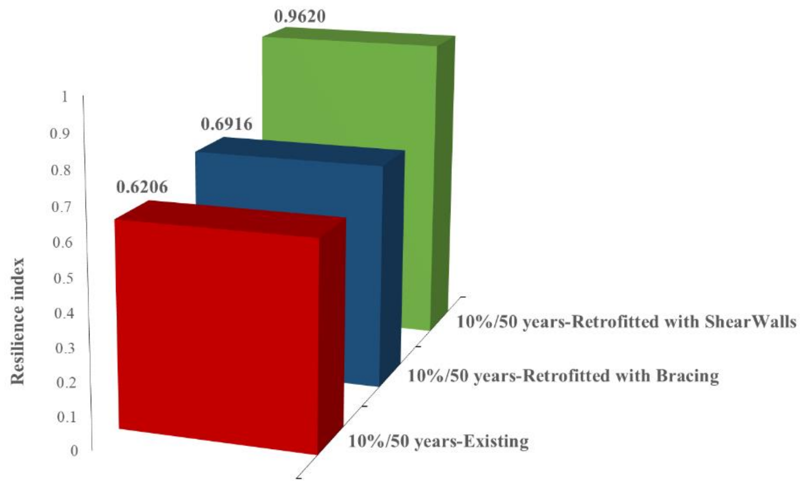

(a)

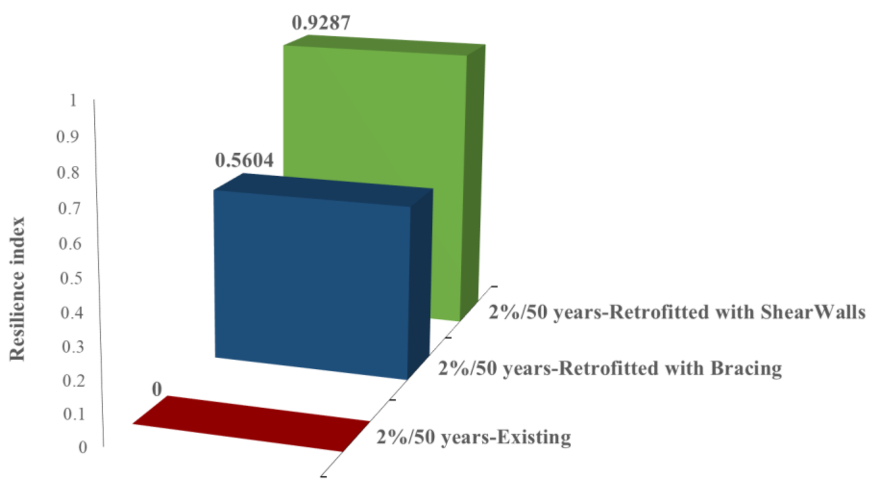

(b)

Fig. 12. Seismic resilience index for the existing school and two retrofitting options under the effect of the mainshock; (a) in hazard level one (10%/50 years); (b) in hazard level two (2%/50 years)

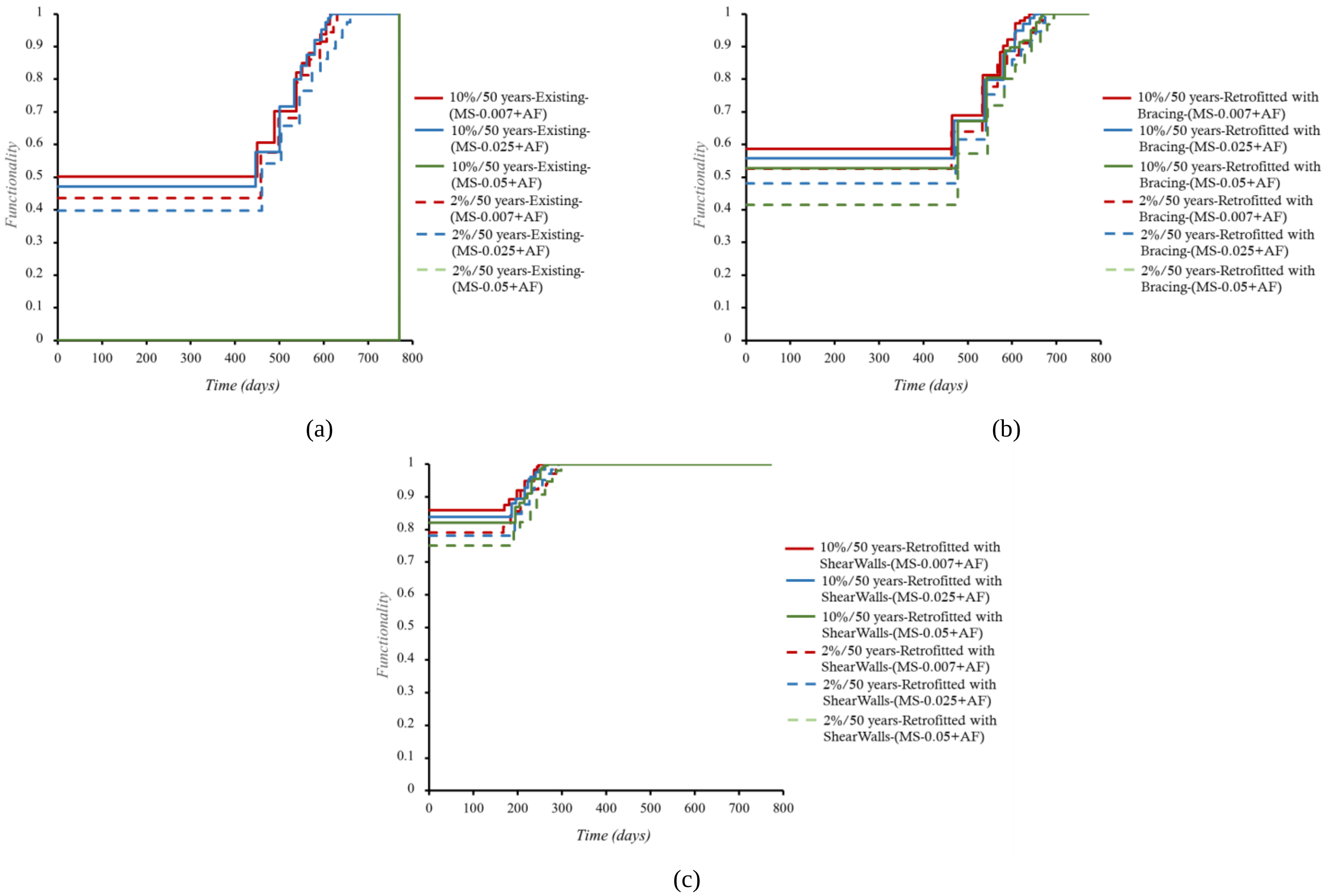

Fig. 13. Functionality curves for the existing school and two retrofitting options under different scenarios of MS-AS.

Table. 12. Seismic resilience index for the existing school and two retrofitting options under different scenarios of MS-AS.

Scenarios of MainShok-AfterShock	Seismic Hazard Level	Resilience Index		
		Existing School	Retrofitted with Bracing	Retrofitted with ShearWalls
MS-0.007+AS	1	0.6593	0.7088	0.9616
	2	0.6116	0.6597	0.9393
MS-0.025+AS	1	0.6400	0.6848	0.9545
	2	0.5756	0.6218	0.9349
MS-0.05+AS	1	0	0.6605	0.9480
	2	0	0.5696	0.9226

It is concluded from the previous sections if the intensity of the mainshock increases, the amount of total damage after applying aftershocks will increase, but the retrofitting operation causes that the initial damage produced by the mainshock, which is expressed in terms of MID in this study, does not have a significant effect on the resilience index of the structure under different scenarios of MS-AS. The seismic resilience index for the existing school and retrofitting options under different scenarios of MS-AS is shown in **Fig. 14**. To avoid repetition, the results for the second hazard level (2%/50 years) are shown in **Fig. 14**.

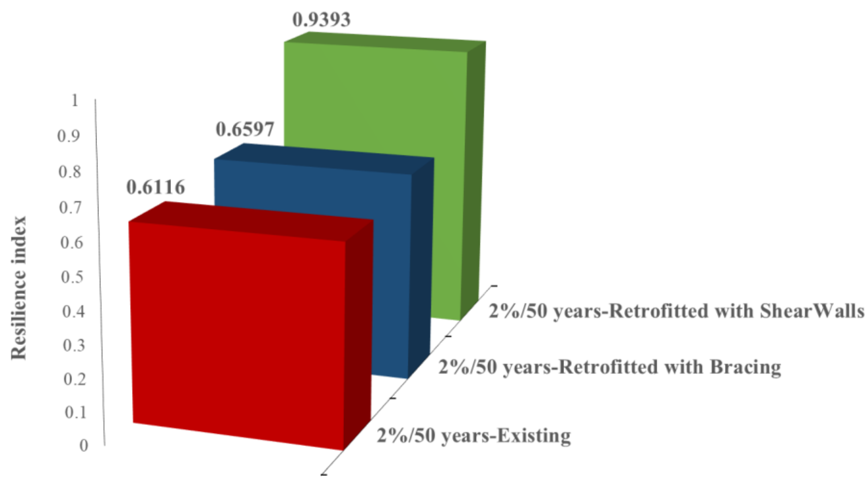

(a)

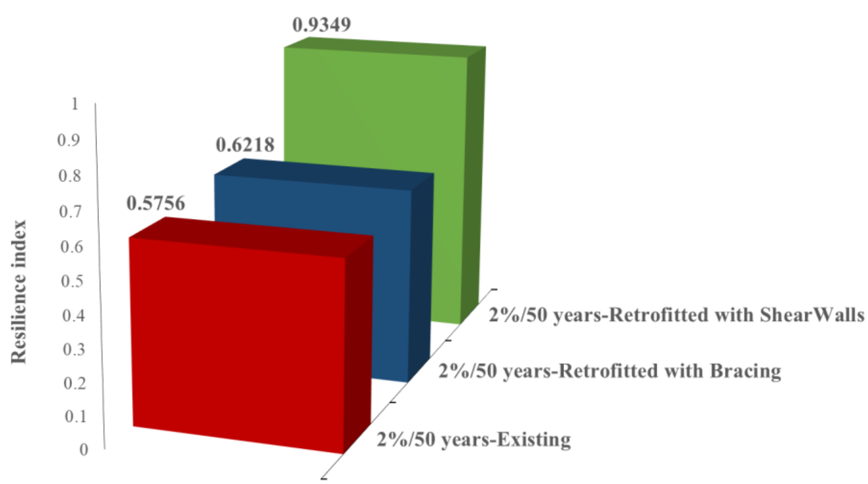

(b)

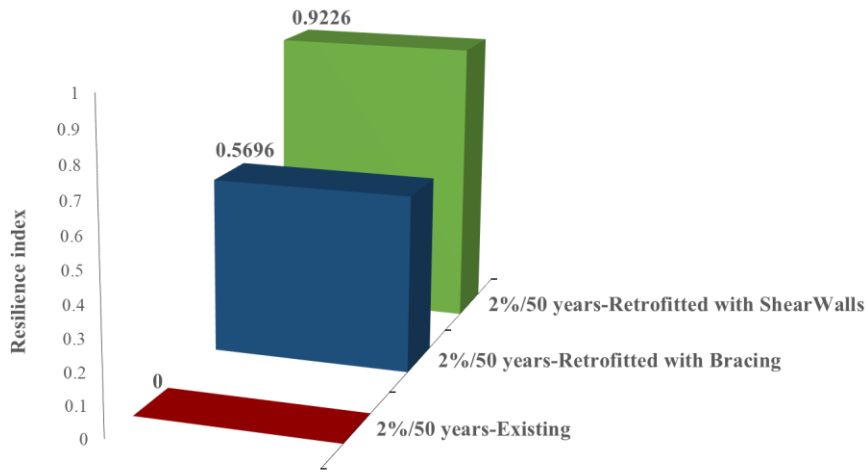

(c)

Fig. 14. The seismic resilience index for the existing school and two retrofitting options under different scenarios of MS-AS: (a) MS-0.007+AS; (b) MS-0.025+AS; (c) MS-0.05+AS

7. Conclusion

In this paper, the selection of the appropriate retrofitting option for a steel school building using the resilience index and FEMA P-58 methodology under the effect of the mainshock and different scenarios of mainshock-aftershock has been presented. A typical Iranian high school and its two retrofitting options have been selected for seismic resilience evaluation at two hazard levels including 10% and 2% in 50 years. The repair time and repair cost of schools after a seismic event are obtained using PACT software. The results show that the damage has increased in all three schools at a hazard level of 2% in 50 years, so the resilience indexes at this hazard level are smaller than another hazard level. The existing school has completely collapsed at 2% in 50 years hazard level under the effect of the mainshock because this school has a weak lateral bearing system and was not designed for this hazard level. In this study, the resilience index of the existing school at hazard level 1 has increased from 0.6206 to 0.6916 for the retrofitting with concentric braces and to 0.9620 for shear walls, respectively. Also, at hazard level 2, the resilience index of the existing school has increased from zero to 0.5604 and 0.9287 in retrofitting options with concentric braces and shear walls, respectively. This increase in the resilience indexes shows the positive effect of retrofitting on the seismic performance of the schools. In this study, to consider mainshock-aftershock sequences, the effect of mainshock damage on the structure before applying the aftershocks has been evaluated. To indicate the mainshock damage, the response levels of 0.007, 0.025, and 0.05 maximum inter-story drift values have been considered. From the investigation of the effect of initial damage caused by the mainshock, it is concluded that whatever the intensity of the mainshock increases, the amount of total damage after applying aftershocks will increase, but the retrofitting operation will lead to the initial damage produced by the mainshock does not have any significant effect on the resilience index of the structure under different scenarios of MS-AS.

It is concluded from this study that the retrofitted school with shear walls has experienced less damage at both hazard levels under the effect of the mainshock and different scenarios of mainshock-aftershock, so it has a higher level of resiliency. Also in this retrofitting option, the recovery process is completed in a shorter time and it has a lower repair cost. Therefore, this option is more suitable in terms of economy, construction time, and implementation methods than the other option and is selected as an appropriate option for retrofitting this high school.

As mentioned in the previous sections, the consequence functions for the repair cost provided by the FEMA P-58 methodology were developed based on the construction costs of a specific region (Northern California) and a specific time (2011). Therefore, based on this study, it is suggested that fragility curves related to structural and non-structural components based on the components used in Iran should be developed in the PACT Library to assess the seismic damage of Iranian schools using FEMA P-58 methodology. In this case, the obtained results will be more accurate and more consistent with reality.

Appendix A.

The plan of the beams of the floors. (**Fig. A1**)

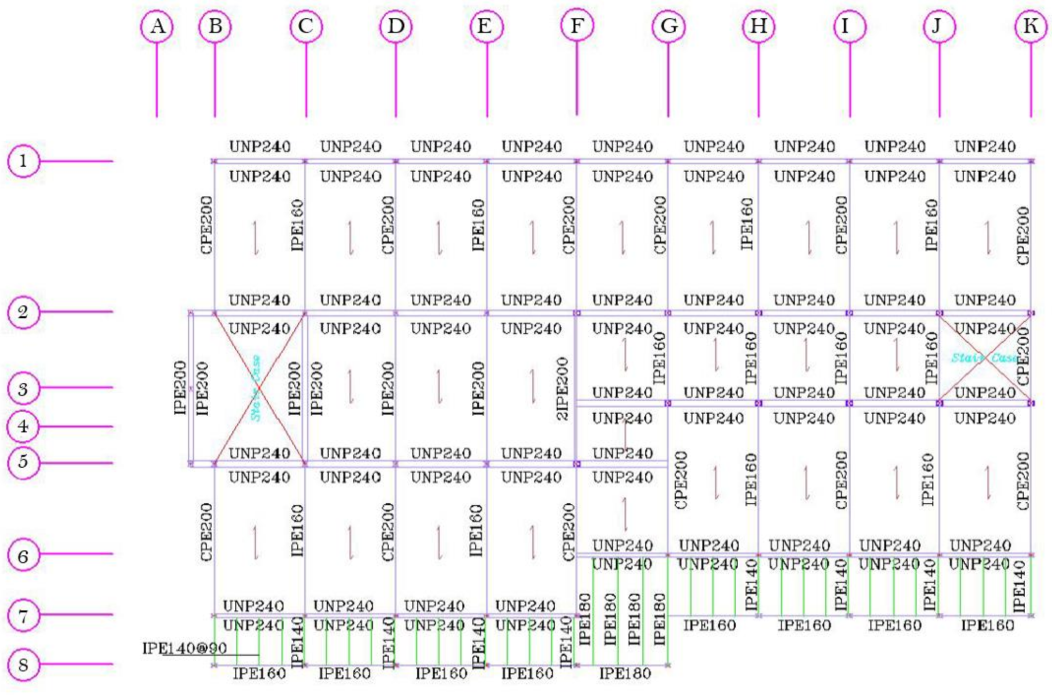

(a)

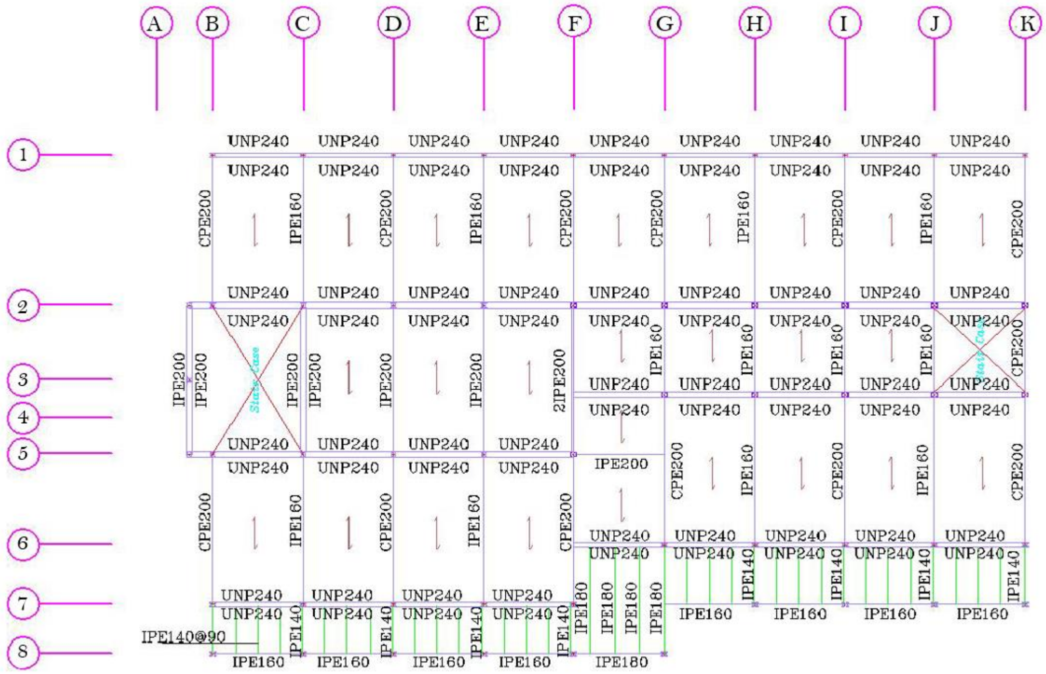

(b)

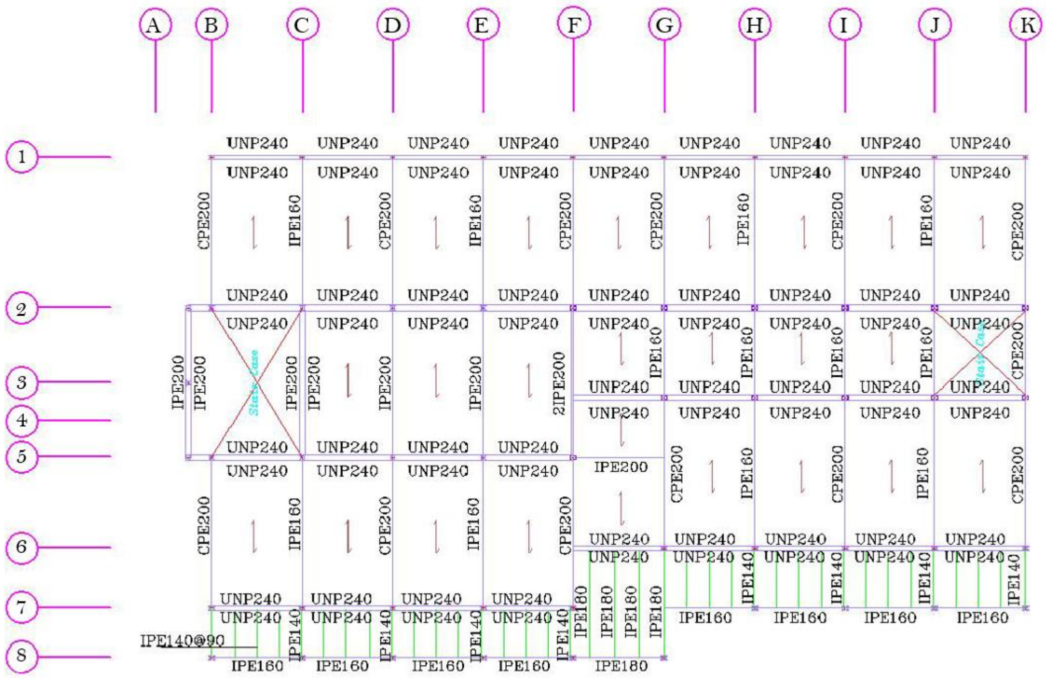

(c)

Fig. A1. The plan of the beams: (a) at the first story; (b) second story (c) third story

Appendix B.

The characteristics of the selected records. (**Table. B1**)

Table. B1. Selected ground motions for performing IDA.

No.	Type	Earthquake	Magnitude	Record name	Station name	Database
1	MS	Coalinga	6.36	NGA_no_368_A-PVY045.AT2	PLEASANT VALLEY P.P. – YARD	PEER NGA
	AS		5.09	NGA_no_383_A-PVY045.AT2		
2	MS	Coalinga	6.36	NGA_no_368_H-PVY135.AT2	PLEASANT VALLEY P.P. – YARD	PEER NGA
	AS		5.09	NGA_no_383_A-PVY135.AT2		
3	MS	Chalfant Valley	6.19	ChalfantValley86_CE54171P.V2	NO. 54171	CESMD
	AS		5.44	ChalfantValley86C_CE54171P.V2		
4	MS	Chalfant Valley	6.19	ChalfantValley86_CE54428P.V2	NO.54428	CESMD
	AS		5.44	ChalfantValley86B_CE54428P.V2		
5	MS	Chalfant Valley	6.19	ChalfantValley86_CE54424P.V2	NO.54424	CESMD
	AS		5.44	ChalfantValley86B_CE54424P.V2		
6	MS	Imperial Valley	6.53	NGA_no_162_H-CXO315.AT2	CALEXICO FIRE STA	PEER NGA
	AS		5.01	NGA_no_195_A-CXO315.AT2		
7	MS	Imperial Valley	6.53	NGA_no_174_H-E11140.AT2	EL CENTRO ARRAY 11	PEER NGA
	AS		5.01	NGA_no_199_A-E11140.AT2		
8	MS	Imperial Valley	6.53	NGA_no_178_H-E03230.AT2	EL CENTRO ARRAY 3	PEER NGA
	AS		5.01	NGA_no_201_A-E03230.AT2		
9	MS	Imperial Valley	6.53	NGA_no_172_H-E01230.AT2	EL CENTRO ARRAY 1	PEER NGA
	AS		5.01	NGA_no_197_A-E01230.AT2		
10	MS	Imperial Valley	6.53	NGA_no_169_H-DLT262.AT2	DELTA	PEER NGA
	AS		5.01	NGA_no_196_A-DLT262.AT2		
11	MS	Livermore	5.8	Livermore80A_CE57187P.V2	NO.57187	CESMD
	AS		5.42	Livermore80B_CE57187P.V2		
12	MS	Livermore	5.8	Livermore80A_CE67070P.V2	NO. 67070	CESMD
	AS		5.42	Livermore80B_CE67070P.V2		
13	MS	Livermore	5.8	NGA_no_212_A-DVD246.AT2	DEL VALLE DAM	PEER NGA
	AS		5.42	NGA_no_219_B-DVD246.AT2		
14	MS	Livermore	5.8	NGA_no_214_A-KOD180.AT2	SAN RAMON KODAK BLDG	PEER NGA
	AS		5.42	NGA_no_223_B-KOD180.AT2		
15	MS	Livermore	5.8	NGA_no_215_A-SRM070.AT2	SAN RAMON	PEER NGA
	AS		5.42	NGA_no_224_B-SRM070.AT2		
16	MS	Livermore	5.8	NGA_no_213_A-FRE075.AT2	FREMONT MISSION S.J.	PEER NGA
	AS		5.42	NGA_no_220_B-FRE075.AT2		

17	MS	Livermore	5.8	NGA_no_210_A-A3E236.AT2	HAYWARD CSUH STADIUM	PEER NGA
	AS		5.42	NGA_no_217_B-A3E236.AT2		
18	MS	Mammoth Lakes	6.06	NGA_no_231_I-LUL090.AT2	LONG VALLEY DAM UPR L	PEER NGA
	AS		5.94	NGA_no_250_L-LUL090.AT2		
19	MS	Mammoth Lakes	6.06	NGA_no_231_I-LUL090.AT2	LONG VALLEY DAM UPR L	PEER NGA
	AS		5.7	NGA_no_243_B-LUL090.AT2		
20	MS	Mammoth Lakes	6.06	NGA_no_231_I-LUL090.AT2	LONG VALLEY DAM UPR L	PEER NGA
	AS		5.69	NGA_no_234_J-LUL090.AT2		
21	MS	Northridge	6.69	NGA_no_963_ORR090.AT2	CASTAIC - OLD RIDGE ROUTE	PEER NGA
	AS		5.93	NGA_no_1676_CASTA090.AT2		
22	MS	Northridge	6.69	NGA_no_1039_MRP090.AT2	MOORPARK	PEER NGA
	AS		5.93	NGA_no_1681_MPARK090.AT2		
23	MS	Northridge	6.69	NGA_no_1005_TEM090.AT2	LOS ANGELES - TEMPLE & HOPE	PEER NGA
	AS		5.28	NGA_no_1712_TEMPL090.AT2		
24	MS	Northridge	6.69	NGA_no_971_ELI180.AT2	ELIZABETH LAKE	PEER NGA
	AS		5.93	NGA_no_1677_ELIZL180.AT2		
25	MS	Northridge	6.69	NGA_no_945_ANA180.AT2	ANAVERDE VALLEY - CITY RANCH	PEER NGA
	AS		5.93	NGA_no_1675_ANAVE180.AT2		
26	MS	Northridge	6.69	NGA_no_990_LAC180.AT2	LOS ANGELES - CITY TERRACE	PEER NGA
	AS		5.93	NGA_no_1678_CTYTE180.AT2		
27	MS	Northridge	6.69	NGA_no_1007_UNI095.AT2	LA-UNIV. HOSPITAL GR	PEER NGA
	AS		5.93	NGA_no_1680_UNIHP090.AT2		
28	MS	Petrolia	7.2	Petrolia_25Apr1992_CE89530P.V2	NO. 89530	CESMD
	AS		6.7	PetroliaAftershock2_26Apr1992_CE89530P.V2		
29	MS	Petrolia	7.2	Petrolia_25Apr1992_CE89156P.V2	NO. 89156	CESMD
	AS		6.5	PetroliaAftershock1_26Apr1992_CE89156P.V2		
30	MS	Petrolia	7.2	Petrolia_25Apr1992_CE89509P.V2	NO. 89509	CESMD
	AS		6.5	PetroliaAftershock1_26Apr1992_CE89509P.V2		
31	MS	Whittier Narrows	5.99	NGA_no_615_A-DWN270.AT2	DOWNEY	PEER NGA
	AS		5.27	NGA_no_709_B-DWN270.AT2		
32	MS	Whittier Narrows	5.99	NGA_no_663_A-MTW000.AT2	MT WILSON	PEER NGA
	AS		5.27	NGA_no_715_B-MTW000.AT2		

Appendix C

Table. C1. Components and their quantities for all three types of schools.

Fragility ID	Component Description per FEMA P-58	Units	Location (Floor)	Quantity per Direction			EDP
				N-S	E-W	ND	
[a]B1033.073a	Braced frame, design for factored loads, no additional seismic detailing, X Brace, Brace w < 40 PLF	EA	1	8	4	-	SDR
			2	8	4	-	
			3	8	4	-	
[b]B1033.053a	Ordinary Concentric Braced Frame w compact braces, X Brace, Brace w < 40 PLF	EA	1	10	9	-	SDR
			2	10	9	-	
			3	7	5	-	
[c]B1044.011	Rectangular low aspect ratio concrete walls 8"-16" double curtain; with heights of up to 15'	144 SF	1	7.27	-	-	SDR
			2	7.27	-	-	
			3	7.27	-	-	
[c]B1044.071	Low rise reinforced concrete walls with boundary columns, 8" to 16" thick, height <15'	144 SF	1	-	5.02	-	SDR
			2	-	5.02	-	
			3	-	5.02	-	
B1071.041	Exterior Wall - Type: Gypsum with wood studs, Full Height, Fixed Below, Fixed Above	100 LF	1	1.32	2.17	-	SDR
			2	1.32	2.17	-	
			3	1.32	2.17	-	
C1011.001a	Wall Partition, Type: Gypsum with metal studs, Full Height, Fixed Below, Fixed Above	100 LF	1	1.79	2.86	-	SDR
			2	1.59	2.99	-	
			3	1.39	2.99	-	
C2011.031b	Hybrid stair assembly with steel stringers and concrete treads and landings with no seismic joints.	EA	1	2	-	-	SDR
			2	2	-	-	
			3	2	-	-	
C3011.002a	Wall Partition, Type: Gypsum + Ceramic Tile, Full Height, Fixed Below, Fixed Above	100 LF	1	0.79	2.86	-	SDR
			2	0.39	2.99	-	
			3	0.39	2.99	-	
C3032.001d	Suspended Ceiling, SDC A, B, C, Area (A): A > 2500, Vert support only	2500 SF	1	-	-	2.76	PFA
			2	-	-	2.76	
			3	-	-	2.76	

*The quantity of components: B1071.041, C1011.001a, C2011.031b, C3011.002a and C3032.001d are considered similar for all three schools.
EDP = Engineering Demand Parameter; N-S = North-South Direction; E-W=East-West Direction; ND = Nondirectional
SF = Square Feet; EA = Each; LF = Linear Foot
SDR = Story Drift Ratio; PFA = Peak Floor Acceleration (g)
a) Only for Existing School.
b) Only for Retrofitted with Bracing.
c) Only for Retrofitted with Shear Walls.

References:

Almufti, I., & Willford, M. (2013). REDi™ rating system: Resilience-based earthquake design initiative for the next generation of buildings. Arup Co.

ASCE-41. (2006). Seismic rehabilitation of existing buildings, American Society of Civil Engineers, Reston, VA.

Baker, J. W., Cremen, G., Giovinazzi, S., & Seville, E. (2016). Benchmarking FEMA P-58 performance predictions against observed earthquake data-A preliminary evaluation for the Canterbury earthquake sequence. In Proceedings of the 2016 Annual Conference of the New Zealand Society for Earthquake Engineering, Christchurch, New Zealand.

Bruneau, M., Chang, S. E., Eguchi, R. T., Lee, G. C., O'Rourke, T. D., Reinhorn, A. M., ... & Von Winterfeldt, D. (2003). A framework to quantitatively assess and enhance the seismic resilience of communities. Earthquake Spectra, 19(4), 733-752.

Building and Housing Research Center (BHRC). Iranian code of practice for seismic resistant design of buildings." (standard no. 2800). 4th edition, Tehran, Iran. 2015.

CESMD (Center for Engineering Strong Motion Data). http://www.strongmotioncenter.org/. Last access: 04/24/2013.

Chang, S. E., & Shinozuka, M. (2004). Measuring improvements in the disaster resilience of communities. Earthquake Spectra, 20(3), 739-755.

Cimellaro, G. P., & Piqué, M. (2016). Resilience of a hospital emergency department under seismic event. Advances in Structural Engineering, 19(5), 825-836.

Cimellaro, G. P., Reinhorn, A. M., & Bruneau, M. (2010). Framework for analytical quantification of disaster resilience. Engineering structures, 32(11), 3639-3649.

Cimellaro, G. P., Renschler, C., Reinhorn, A. M., & Arendt, L. (2016). PEOPLES: a framework for evaluating resilience. Journal of Structural Engineering, 142(10), 04016063.

D'Ayala D., Faure-Walker, J., Mildon, Z., Lombardi, D., Galasso, C., Pedicone, D., Putrino, V., Perugini, P., De Luca, F., Del Gobbo, G., Lloyd, T., Morgan, E., Totaro, A., Alexander, D., Tagliacozzo, S., (2016) The Mw 6.2 Earthquake of 24th of August 2016. A field report by EEFIT, available at https://www.istructe.org/resources-centre/technical-topicareas/eefit/eefit-reports, 2019.

D'Ayala, D., Galasso, C., Nassirpour, A., Adhikari, R. K., Yamin, L., Fernandez, R., ... & Oreta, A. (2020). Resilient communities through safer schools. International journal of disaster risk reduction, 45, 101446.

De Angelis, A., & Pecce, M. (2015). Seismic nonstructural vulnerability assessment in school buildings. Natural Hazards, 79(2), 1333-1358.

De Martino, G., Di Ludovico, M., Prota, A., Moroni, C., Manfredi, G., & Dolce, M. (2017). Estimation of repair costs for RC and masonry residential buildings based on damage data collected by post-earthquake visual inspection. Bulletin of Earthquake Engineering, 15(4), 1681-1706.

Dolsek, M., & Fajfar, P. (2005). Simplified non-linear seismic analysis of infilled reinforced concrete frames. Earthquake engineering & structural dynamics, 34(1), 49-66.

DRES; the organization for Development, Renovation and Equipping Schools of Iran, https://dres.ir/fa, 2020

Eghbali, M., Samadian, D., Ghafory-Ashtiany, M., & Dehkordi, M. R. (2020). Recovery and reconstruction of schools after M 7.3 Ezgeleh-Sarpole-Zahab earthquake; part II: Recovery process and resiliency calculation. Soil Dynamics and Earthquake Engineering, 139, 106327.

Ekhlaspoor, A., Raissi Dehkordi, M., Eghbali, M., & Samadian, D. (2022). Pre-event assessment of seismic resilience index for typical Iranian buildings via a web-based tool. International Journal of Civil Engineering, 20(3), 257-272.

Federal Emergency Management Agency (FEMA). FEMA P-58-1: Seismic performance assessment of buildings, volume 1–methodology. Washington, DC: Federal Emergency Management Agency; 2018a.

Federal Emergency Management Agency (FEMA). FEMA P-58-2: Performance Assessment Calculation Tool (PACT). Washington, DC: Federal Emergency Management Agency; 2018b.

FEMA. Techniques for the seismic rehabilitation of existing buildings vol. 547. Washington, DC: FEMA; 2007.

Gogus, A. (2010). Structural wall systems-nonlinear modeling and collapse assessment of shear walls and slab-column frames. A dissertation submitted in partial satisfaction of the requirements for the degree Doctor of Philosophy in Civil Engineering, UNIVERSITY OF CALIFORNIA Los Angeles.

Gogus, A., & Wallace, J. W. (2015). Seismic safety evaluation of reinforced concrete walls through FEMA P695 methodology. Journal of Structural Engineering, 141(10), 04015002.

Gunnarsson, I. R. (2004). Numerical performance evaluation of braced frame systems (Doctoral dissertation, University of Washington).

Han, R., Li, Y., & van de Lindt, J. (2014). Seismic risk of base isolated non-ductile reinforced concrete buildings considering uncertainties and mainshock–aftershock sequences. Structural Safety, 50, 39-56.

Home III, J. F., & Orr, J. E. (1997). Assessing behaviors that create resilient organizations. Employment Relations Today, 24(4), 29-39.

Hosseinzadeh, S., & Galal, K. (2020a). System-level seismic resilience assessment of reinforced masonry shear wall buildings with masonry boundary elements. In Structures (Vol. 26, pp. 686-702). Elsevier.

Hosseinzadeh, S., & Galal, K. (2020b). Seismic fragility assessment and resilience of reinforced masonry flanged wall systems. Journal of Performance of Constructed Facilities, 34(1), 04019109.

Jalali, S. A., Amini, A., Mansouri, I., & Hu, J. W. (2021). Seismic collapse assessment of steel plate shear walls considering the mainshock–aftershock effects. Journal of Constructional Steel Research, 182, 106688.

Joyner, M. D., & Sasani, M. (2020). Building performance for earthquake resilience. Engineering Structures, 210, 110371.

Kendra, J. M. Wachtendorf T (2003). Elements of resilience after the World Trade Center Disaster: reconstituting New York City's Emergency Operations Centre. Disasters, 27(1), 37-53.

Klein, R. J. T., Nicholls, R. J., & Thomalla, F. (2003). Resilience to natural hazards: How useful is this concept? Environ Hazards 5:35–45. https://doi.org/10.1016/j.hazards.2004.02.001

Kurth, M. H., Keenan, J. M., Sasani, M., & Linkov, I. (2019). Defining resilience for the US building industry. Building Research & Information, 47(4), 480-492.

Li, Y., Song, R., & Van De Lindt, J. W. (2014). Collapse fragility of steel structures subjected to earthquake mainshock-aftershock sequences. Journal of Structural Engineering, 140(12), 04014095.

McKenna F, Fenves GL (2020). Open system for earthquake engineering simulation, version 3.2.0." pacific earthquake engineering research center. Berkeley, CA: Univ. of California.

Miranda, E., Mosqueda, G., Retamales, R., & Pekcan, G. (2012). Performance of nonstructural components during the 27 February 2010 Chile earthquake. Earthquake Spectra, 28(1_suppl1), 453-471.

Mokhtari, M., & Naderpour, H. (2020). Seismic resilience evaluation of base-isolated RC buildings using a loss-recovery approach. Bulletin of Earthquake Engineering, 18(10), 5031-5061.

Naderpour, H., & Vakili, K. (2019). Safety assessment of dual shear wall-frame structures subject to Mainshock-Aftershock sequence in terms of fragility and vulnerability curves. Earthquakes and Structures, 16(4), 425-436.

Niazi, M., Dehkordi, M. R., Eghbali, M., & Samadian, D. (2021). Seismic resilience index evaluation for healthcare facilities: a case study of hospital in Tehran. International Journal of Disaster Risk Reduction, 65, 102639.

Odabaşi, Ö., Kohrangi, M., Fagà, E., & Bazzurro, P. (2020). Consequence Functions for Seismic Risk Assessment: A review of consequence modeling state-of-practice for ERM-CH– Module D.

Pacific Earthquake Engineering Research Center PEER Ground Motion Database. http://peer.berkeley.edu/peer_ground_motion_database. Last access: 04/20/2013.

Paton, D., Smith, L., & Violanti, J. (2000). Disaster response: risk, vulnerability and resilience. Disaster Prevention and Management: An International Journal, 9(3), 173-180.

Perrone, D., O'Reilly, G. J., Monteiro, R., & Filiatrault, A. (2020). Assessing seismic risk in typical Italian school buildings: From in-situ survey to loss estimation. International journal of disaster risk reduction, 44, 101448.

Putrino, V., & D'Ayala, D. (2019). Norcia and Amatrice. A comparison of the two historic centers' performance under the Central Italy earthquake sequence Proceedings of the 7th ECCOMAS Thematic Conference on Computational Methods in Structural Dynamics and Earthquake Engineering, pp. 2636-2648

Rajabpour, N. (2018). Evaluation of seismic resilience index and sensitivity analysis of existing steel moment resisting frames using fragility and vulnerability curves, A Thesis Submitted in Partial Fulfillment of the Requirement for the Degree of Master of Science in Civil Engineering.

Ranjbar, P. R., & Naderpour, H. (2020). Probabilistic evaluation of seismic resilience for typical vital buildings in terms of vulnerability curves. In Structures (Vol. 23, pp. 314-323). Elsevier.

Renschler, C., Reinhorn, A. M., Arendt, L., & Cimellaro, G. P. (2011). The PEOPLES Resilience Framework: A conceptual approach to quantify community resilience. Proceedings of COMPDYN, 26-28.

Risk Management Series. FEMA P-424, Design Guide - for Improving School Safety in Earthquakes, Floods, and High Winds, 2010

Ruiz-García, J., Olvera, R. N., & Frías, A. D. (2021). Seismic assessment of school buildings with short captive RC columns under subduction seismic sequences. In Structures (Vol. 34, pp. 2432-2444). Elsevier.

Samadian, D., Eghbali, M., Dehkordi, M. R., & Ghafory-Ashtiany, M. (2020). Recovery and reconstruction of schools after M 7.3 Ezgeleh-Sarpole-Zahab earthquake of Nov. 2017; part I: Structural and nonstructural damages after the earthquake. Soil Dynamics and Earthquake Engineering, 139, 106305.

Samadian, D., Ghafory-Ashtiany, M., Naderpour, H., & Eghbali, M. (2019). Seismic resilience evaluation based on vulnerability curves for existing and retrofitted typical RC school buildings. Soil Dynamics and Earthquake Engineering, 127, 105844.

Sardari, F., Raissi-Dehkordi, M., Eghbali, M., & Samadian, D. (2020). Practical seismic retrofit strategy based on reliability and resiliency analysis for typical existing steel school buildings in Iran. International Journal of Disaster Risk Reduction 51(C):101890

Scholz, C. H. (2002). The mechanics of earthquakes and faulting, Cambridge University Press, Cambridge, U.K.

Shamsoddini-Motlagh, Z., Raissi-Dehkordi, M., Eghbali, M., & Samadian, D. (2020). Evaluation of seismic resilience index for typical RC school buildings considering carbonate corrosion effects. International journal of disaster risk reduction, 46, 101511.

Terzic, V., Kolozvari, K., & Saldana, D. (2019). Implications of modeling approaches on seismic performance of low-and mid-rise office and hospital shear wall buildings. Engineering Structures, 189, 129-146.

Terzic, V., Villanueva, P. K., Saldana, D., & Yoo, D. Y. (2021). F-Rec Framework: Novel framework for probabilistic evaluation of functional recovery of building systems. PEER Report, 6.

Vamvatsikos, D., & Cornell, C. A. (2001). Tracing and post-processing of IDA curves: Theory and software implementation. Report No. RMS, 44.

Vamvatsikos, D., & Cornell, C. A. (2002). Incremental dynamic analysis. Earthquake engineering & structural dynamics, 31(3), 491-514.

Van der Leeuw, S. E., & Aschan-Leygonie, C. (2005). A long-term perspective on resilience in socio-natural systems. Micro-Meso-Macro: Addressing Complex Systems Couplings, London, World Scientific, 227-264.

Vatteri, A. P., D 'Ayala, D., & Gehl, P. (2022). Bayesian networks for assessment of disruption to school systems under combined hazards. International Journal of Disaster Risk Reduction, 74, 102924.

Wen, W., Zhang, M., Zhai, C., & Liu, W. (2019). Resilience loss factor for evaluation and design considering the effects of aftershocks. Soil Dynamics and Earthquake Engineering, 116, 43-49.